

Stabilized low-order finite element approximation for linear three-field poroelasticity

Lorenz Berger¹, Rafel Bordas¹, David Kay¹, and Simon Tavener²

¹Department of Computer Science, University of Oxford

²Department of Mathematics, Colorado State University

December 2013

Abstract

A stabilized conforming finite element method for the three-field (displacement, fluid flux and pressure) poroelasticity problem is presented. We use the lowest possible approximation order: piecewise constant approximation for the pressure, and piecewise linear continuous elements for the displacements and fluid flux. By applying a local pressure jump stabilization term to the mass conservation equation we avoid pressure oscillations and the discretization leads to a symmetric linear system. For the fully discretized problem we prove existence and uniqueness, an energy estimate and an optimal a-priori error estimate, including an error estimate for the fluid flux in its natural $Hdiv$ norm. Numerical experiments in 2D and 3D illustrate the convergence of the method, show the effectiveness of the method to overcome spurious pressure oscillations, and evaluate the added mass effect of the stabilization term.

1 Introduction

Poroelasticity is a simplified mixture theory in which a complex fluid-structure interaction problem is approximated by a superposition of both solid and fluid components using averaging techniques. In this work we assume small deformations allowing us to significantly simplify the equations. A detailed discussion and derivation of the general equations can be found in the standard Poromechanics book by Coussy [12].

Biot's poroelastic theory has been used in various geomechanical applications ranging from reservoir engineering [30] to modelling earthquake fault zones [39]. More recently, fully saturated incompressible poroelastic models, often derived using the theory of mixtures [7], have been used for modelling biological tissues. For example, modelling lung parenchyma [23], protein based hydrogels embedded within cells [17], perfusion of blood flow in the beating myocardium [10],[11], the modelling of brain oedema [25] and hydrocephalus [41], along with the modelling of interstitial fluid and tissue in articular cartilage and intervertebral discs [28],[19],[16]. In this work, we focus on the application of modelling biological tissues, and will therefore restrict the equations to the

fully saturated incompressible case. By doing so we reduce the workings, and still retain all the numerical difficulties associated with solving the full Biot model, some of which are discussed next.

After many decades of research there remain numerous challenges associated with the numerical solution of the poroelastic equations. When using the finite element method the main challenge is to ensure stability and convergence of the method and prevent numerical instabilities that often manifest themselves in the form of oscillations in the pressure. It has been shown that this problem is caused by the saddle point structure in the coupled equations resulting in a violation of the famous Ladyzhenskaya-Babuska-Brezzi (LBB) condition [18], which highlights the need for a stable combination of mixed finite elements. Another numerical challenge in practical 3D applications is the algebraic system arising from the finite element discretisation. This can lead to a very large matrix system that has many unknowns and is severely ill-conditioned, making it difficult to solve using standard iterative based solvers. Therefore low-order finite element methods that reduce the number of degree of freedoms and allow for efficient preconditioning are preferred [40],[15].

The equations are often solved in a reduced displacement and pressure formulation, from which the fluid flux can then be recovered [29],[39]. Murad et. al. [29] have analysed the stability and convergence of this reduced displacement pressure (\mathbf{u}/p) formulation and were able to show error bounds for inf-sup stable combinations of finite element spaces (e.g. Taylor-Hood elements). In this paper we will keep the fluid flux variable resulting in a three-field, displacement, fluid flux, and pressure formulation. Keeping the fluid flux as a primary variable allows for greater accuracy in the velocity field. This can be of interest whenever a consolidation model is coupled with an advection diffusion equation, e.g. to account for thermal effects, contaminant transport or the transport of nutrients or drugs within a porous tissue. Using a three-field formulation also avoids the calculation of the fluid flux in post-processing. Also, when modelling the interaction between a fluid and a poroelastic structure it is important to retain the fluid flux variable to be able to apply physically meaningful boundary conditions at the interface [4]. Another reason for having the fluid flux as a primary variable is that it allows for an easy extension of the fluid model from a Darcy to a Brinkman flow model, for which there are numerous applications in modelling biological tissues [20]. Phillips et. al. [30],[31], have proved error estimates for solving the three-field formulation problem using continuous piecewise linear approximations for displacements and mixed low-order Raviart Thomas elements for the fluid flux and pressure variables. In [24], a discontinuous method and in [42] a nonconforming three-field method is analysed. These papers are motivated by the need for a method that is able to overcome pressure oscillations (see [33]) experienced by the method in Phillips et. al. [30],[31]. In addition to these monolithic approaches there has been considerable work on operating splitting (iterative) approaches for solving the poroelastic equations [38],[14],[21]. Although these methods are often able to take advantage of existing elasticity and fluid finite element software, and result in solving a smaller system of equations, these schemes are often only conditionally stable. To ensure that the method is unconditionally stable monolithic approaches are often preferred. The method proposed in this work is monolithic, and will therefore retain the advantage of being unconditionally stable.

To satisfy the LBB condition numerous stabilization techniques for finite element methods have already been proposed, most extensively for the model equations of Stokes and Darcy flow, which despite their simplicity retain all the difficulties of a constraint problem. A good introduction on stabilization techniques for the Stokes problem can be found in chapter 5 of [13]. For a comparison of low-order stabilization techniques for the Darcy problem we refer to [6]. Most stabilized methods lead to a modified variational formulation in which an additional term is added to the mass bal-

ance equation, modifying the incompressibility constraint in such a way that stability of the mixed formulation is increased, while still maintaining optimal convergence of the method. These stabilization techniques are of great interest to us since solving the three-field poroelasticity problem is essentially equivalent to coupling the Stokes equations (elasticity of the porous mixture) with the Darcy equations (fluid flow through pores), with a modified incompressibility constraint that combines the divergence of the displacement velocity and the fluid flux. In this work we will use the local pressure jump stabilization method [9] that has already successfully been used for solving the Stokes and Darcy equations independently or coupled via an interface. This mixed scheme uses the lowest possible approximation order, piecewise constant approximation for the pressure and piecewise linear continuous elements for the displacement and fluid flux. A motivation for using piecewise constant pressure elements is that in practical scenarios the domain often has large permeability contrasts, and the solution may then contain steep pressure gradients. In this situation continuous pressure elements often struggle to capture the steep gradient at the interface between the high-permeable and low-permeable region, and as a result overshoot the true solution. By using a low-order piecewise constant (discontinuous) approximation for the pressure we can approximate these steep pressure gradients reliably, and avoid localized oscillations in the pressure [39]. There are also other practical advantages from using low-order interpolation elements, such as obtaining a linear system that is smaller relative to accuracy and has less bandwidth, and ease of implementation and discretization of geometrically complicated domains. The resulting linear system is also symmetric and has a nice block structure that is well suited for effective preconditioning.

The rest of this paper is organized as follows: in section 1.1, we describe the model equations; in section 2 we present the continuous weak formulation of the model; in section 3 we introduce the fully-discrete model, prove existence and uniqueness at each time step, and give an energy estimate over time. We then derive an optimal order a-priori error estimate in section 4. Finally in section 5, we present some numerical experiments that verify our theoretical findings in 2D and 3D, test the robustness of the method, and show that it is able to overcome pressure oscillations.

1.1 The model

The governing equations of the Biot model, with the displacement \mathbf{u} , fluid flux \mathbf{z} , and pressure p as primary variables are summarized below:

$$-\nabla \cdot \boldsymbol{\sigma} = \mathbf{f} \quad \text{in } \Omega, \quad (1.1a)$$

$$\boldsymbol{\kappa}^{-1} \mathbf{z} + \nabla p = \mathbf{b} \quad \text{in } \Omega, \quad (1.1b)$$

$$\nabla \cdot \mathbf{z} + \frac{\partial}{\partial t}(\alpha \nabla \cdot \mathbf{u} + c_0 p) = g \quad \text{in } \Omega, \quad (1.1c)$$

$$\mathbf{u}(t) = \mathbf{u}_D \quad \text{on } \Gamma_d, \quad (1.1d)$$

$$\boldsymbol{\sigma}(t) \mathbf{n} = \mathbf{t}_N \quad \text{on } \Gamma_t, \quad (1.1e)$$

$$p(t) = p_D \quad \text{on } \Gamma_p, \quad (1.1f)$$

$$\mathbf{z}(t) \cdot \mathbf{n} = q_D \quad \text{on } \Gamma_f, \quad (1.1g)$$

$$\mathbf{u}(0) = \mathbf{u}^0, \quad p(0) = p^0, \quad \text{in } \Omega, \quad (1.1h)$$

where $\boldsymbol{\sigma}$ is the total stress tensor given by $\boldsymbol{\sigma} = \lambda \text{tr}(\boldsymbol{\epsilon}(\mathbf{u})) \mathbf{I} + 2\mu_s \boldsymbol{\epsilon}(\mathbf{u}) - \alpha p \mathbf{I}$, with the linear strain tensor defined as $\boldsymbol{\epsilon}(\mathbf{u}) = \frac{1}{2} (\nabla \mathbf{u} + (\nabla \mathbf{u})^T)$, g is the fluid source term, \mathbf{f} is the body force on the mixture, and \mathbf{b} is the body force on the fluid. Here Ω is a bounded domain in \mathbb{R}^2 or \mathbb{R}^3 , with

boundary $\partial\Omega = \Gamma_d \cup \Gamma_t$ for the mixture, and $\partial\Omega = \Gamma_p \cup \Gamma_f$ for the fluid, that has an outward pointing unit normal \mathbf{n} . The parameters along with a description are given in Table 1.

Parameter	
Lamé's first parameter	λ ,
Lamé's second parameter (shear modulus)	μ_s ,
Dynamic permeability tensor	$\boldsymbol{\kappa}$,
Solid skeleton density	ρ_s
Fluid density	ρ_f
Biot-Willis constant	α ,
Constrained specific storage coefficient	c_0 .

Table 1: Poroelasticity parameters.

We have also set $\boldsymbol{\kappa} = \mu_f^{-1}\mathbf{k}$, where μ_f and \mathbf{k} are the fluid viscosity and the permeability tensor, respectively. A derivation and more detailed explanation of these equations can be found in [30] and [35]. In this work we will consider a simplification of the full Biot model (1.1), by setting $\alpha = 1$ and $c_0 = 0$. This yields the following fully saturated and incompressible model:

$$-(\lambda + \mu_s)\nabla(\nabla \cdot \mathbf{u}) - \mu_s\nabla^2\mathbf{u} + \nabla p = \mathbf{f} \quad \text{in } \Omega, \quad (1.2a)$$

$$\boldsymbol{\kappa}^{-1}\mathbf{z} + \nabla p = \mathbf{b} \quad \text{in } \Omega, \quad (1.2b)$$

$$\nabla \cdot (\mathbf{u}_t + \mathbf{z}) = g \quad \text{in } \Omega, \quad (1.2c)$$

$$\mathbf{u}(t) = \mathbf{u}_D \quad \text{on } \Gamma_d, \quad (1.2d)$$

$$\boldsymbol{\sigma}(t)\mathbf{n} = \mathbf{t}_N \quad \text{on } \Gamma_t, \quad (1.2e)$$

$$p(t) = p_D \quad \text{on } \Gamma_p, \quad (1.2f)$$

$$\mathbf{z}(t) \cdot \mathbf{n} = q_D \quad \text{on } \Gamma_f, \quad (1.2g)$$

$$\mathbf{u}(0) = \mathbf{u}^0 \quad \text{in } \Omega, \quad (1.2h)$$

The extension of the theoretical results presented in this work to the full Biot equations (1.1), with $\alpha \in \mathbb{R}_{>0}$ and $c_0 \in \mathbb{R}_{>0}$ is straightforward. In the analysis, the constant α would just get absorbed by a general constant C . When $c_0 > 0$, an additional pressure term is introduced into the mass conservation equation. Since this term is coercive, it can only improve the stability of the system.

2 Weak formulation

Before presenting the weak formulation of (1.2), we first need to introduce some notation and bilinear forms. We let $\mathbf{W}^E = \{\mathbf{u} \in H^1(\Omega, \mathbb{R}^d) : \mathbf{u} = \mathbf{u}_D \text{ on } \Gamma_d\}$, $\mathbf{W}^D = \{\mathbf{z} \in H_{div}(\Omega, \mathbb{R}^d) : \mathbf{z} \cdot \mathbf{n} = q_D \text{ on } \Gamma_f\}$. We also define the mixed solution space $\mathcal{W}^X = \{\mathbf{W}^E \times \mathbf{W}^D \times L^2(\Omega)\}$. For the test functions we define the spaces $\mathbf{W}_0^E = \{\mathbf{v} \in H^1(\Omega, \mathbb{R}^d) : \mathbf{v} = 0 \text{ on } \Gamma_d\}$, $\mathbf{W}_0^D = \{\mathbf{w} \in H_{div}(\Omega, \mathbb{R}^d) : \mathbf{w} \cdot \mathbf{n} = 0 \text{ on } \Gamma_f\}$, and $\mathcal{V}^X = \{\mathbf{W}_0^E \times \mathbf{W}_0^D \times L^2(\Omega)\}$. With $\mathbf{u} \in \mathbf{W}^E$ and $\mathbf{v} \in \mathbf{W}_0^E$, we define the bilinear form

$$a(\mathbf{u}, \mathbf{v}) = \int_{\Omega} 2\mu_s(\boldsymbol{\epsilon}(\mathbf{u}) : \boldsymbol{\epsilon}(\mathbf{v})) + \lambda(\nabla \cdot \mathbf{u})(\nabla \cdot \mathbf{v}) \, dx,$$

which corresponds to the elasticity part of the mixture momentum equation (1.2a). This bilinear form is continuous such that

$$a(\mathbf{u}, \mathbf{v}) \leq C_c \|\mathbf{u}\|_{1,\Omega} \|\mathbf{v}\|_{1,\Omega} \quad \forall \mathbf{u}, \mathbf{v} \in H^1(\Omega, \mathbb{R}^d). \quad (2.1)$$

In addition, using Korn's inequality (see 11.2.22 in [8]), and $\int_{\Omega} \lambda(\nabla \cdot \mathbf{v})(\nabla \cdot \mathbf{v}) \geq 0$ we have

$$\|\mathbf{v}\|_{a,\Omega}^2 = a(\mathbf{v}, \mathbf{v}) \geq 2\mu_s \|\epsilon(\mathbf{v})\|_{0,\Omega}^2 \geq C_k \|\mathbf{v}_h\|_{1,\Omega}^2 \quad \forall \mathbf{v} \in \mathbf{W}_0^E. \quad (2.2)$$

We also have

$$\lambda_{min}^{-1} \|\mathbf{w}\|_{0,\Omega}^2 \geq (\boldsymbol{\kappa}^{-1} \mathbf{w}, \mathbf{w}) \geq \lambda_{max}^{-1} \|\mathbf{w}\|_{0,\Omega}^2 \quad \forall \mathbf{w} \in \mathbf{W}_0^D, \quad (2.3)$$

since $\boldsymbol{\kappa}$ is assumed to be a symmetric and positive definite tensor, there exists $\lambda_{min}, \lambda_{max} > 0$ such that $\forall \boldsymbol{\eta} \in \Omega$, $\lambda_{min} \|\boldsymbol{\eta}\|_{0,\Omega} \leq \boldsymbol{\eta}^t \boldsymbol{\kappa}(\mathbf{x}) \boldsymbol{\eta} \leq \lambda_{max} \|\boldsymbol{\eta}\|_{0,\Omega}$ $\forall \boldsymbol{\eta} \in \mathbb{R}^d$, by the boundedness of $\boldsymbol{\kappa}$ [30].

2.1 Continuous weak formulation

We now multiply the strong form of the problem (1.2) by test functions $(\mathbf{v}, \mathbf{w}, q) \in \mathcal{V}^X$ and integrate to yield the continuous weak problem, which is to find $\mathbf{u}(x, t) \in \mathbf{W}^E$, $\mathbf{z}(x, t) \in \mathbf{W}^D$, and $p(x, t) \in L^2$ for any time $t \in [0, T]$ such that:

$$a(\mathbf{u}, \mathbf{v}) - (p, \nabla \cdot \mathbf{v}) = (\mathbf{f}, \mathbf{v}) + (\mathbf{t}_N, \mathbf{v})_{\Gamma_t} \quad \forall \mathbf{v} \in \mathbf{W}_0^E, \quad (2.4a)$$

$$(\boldsymbol{\kappa}^{-1} \mathbf{z}, \mathbf{w}) - (p, \nabla \cdot \mathbf{w}) = (\mathbf{b}, \mathbf{w}) - (p_D, \mathbf{w} \cdot \mathbf{n})_{\Gamma_p} \quad \forall \mathbf{w} \in \mathbf{W}_0^D, \quad (2.4b)$$

$$(\nabla \cdot \mathbf{u}_t, q) + (\nabla \cdot \mathbf{z}, q) = (g, q) \quad \forall q \in L^2. \quad (2.4c)$$

We will assume the following regularity requirements on the data:

$$\mathbf{f} \in C^1([0, T] : (H^{-1}(\Omega))^d), \quad (2.5a)$$

$$\mathbf{b} \in C^1([0, T] : (H_{div}^{-1}(\Omega))^d), \quad (2.5b)$$

$$g \in C^0([0, T] : (L^2(\Omega))^d), \quad (2.5c)$$

$$\mathbf{u}_D \in C^1([0, T] : H^{1/2}(\Gamma_d)), \quad (2.5d)$$

$$\mathbf{t}_N \in C^1([0, T] : H^{-1/2}(\Gamma_t)), \quad (2.5e)$$

$$q_D \in C^0([0, T] : TrW), \quad (2.5f)$$

$$p_D \in C^0([0, T] : L^2(\Gamma_p)), \quad (2.5g)$$

where $TrW := \{\mathbf{w} \cdot \mathbf{n}|_{\Gamma_f} : \mathbf{w} \in (H_{div}(\Omega))^d\}$. For the initial conditions we require that

$$\mathbf{u}^0 \in (H^1(\Omega))^d, \quad \mathbf{z}^0 \in (H_{div}(\Omega))^d, \quad p^0 \in L^2(\Omega). \quad (2.6)$$

3 Fully-discrete model

We begin with some standard finite element notation. Let $\xi_h = \{E_1, E_2, \dots, E_{N_h}\}$ be a subdivision of Ω , where E_j is a d -simplex. Let $h_j = \text{diam}(E_j)$ and set $h = \max\{h_j : j = 1, \dots, M_h\}$. The mixed finite element space defined on ξ_h is given as $\mathcal{W}_h^X = (\mathbf{W}_h^E \times \mathbf{W}_h^D \times Q_h) \subset (\mathbf{W}^E \times \mathbf{W}^D \times L^2(\Omega))$, similarly for the test function we let $\mathcal{V}_h^X = (\mathbf{W}_{h0}^E \times \mathbf{W}_{h0}^D \times Q_h) \subset (\mathbf{W}_0^E \times \mathbf{W}_0^D \times L^2(\Omega))$. We will

now give a conforming mixed finite element method for discretization of (2.4). To discretize the time derivative we use the fully implicit backward Euler scheme, which we will denote using the shorthand $v_{\delta t}^n := \frac{v^n - v^{n-1}}{\Delta t}$. Let \mathbf{u}_h denote the approximate displacement solution over all time steps, such that $\mathbf{u}_h = \{\mathbf{u}_h^0, \mathbf{u}_h^1, \dots, \mathbf{u}_h^n, \dots, \mathbf{u}_h^T\}$, and similarly for the other variables. We also add the pressure jump term $J(p_{\delta t h}, q_h)$ to stabilize the system. The fully discretized weak problem is now to find $\mathbf{u}_h^n \in \mathbf{W}_h^E$, $\mathbf{z}_h^n \in \mathbf{W}_h^D$ and $p_h^n \in Q_h$ such that:

$$a(\mathbf{u}_h^n, \mathbf{v}_h) - (p_h^n, \nabla \cdot \mathbf{v}_h) = (\mathbf{f}^n, \mathbf{v}_h) + (\mathbf{t}_N, \mathbf{v}_h)_{\Gamma_t} \quad \forall \mathbf{v}_h \in \mathbf{W}_{h0}^E, \quad (3.1a)$$

$$(\boldsymbol{\kappa}^{-1} \mathbf{z}_h^n, \mathbf{w}_h) - (p_h^n, \nabla \cdot \mathbf{w}_h) = (\mathbf{b}^n, \mathbf{w}_h) - (p_D, \mathbf{w}_h \cdot \mathbf{n})_{\Gamma_p} \quad \forall \mathbf{w}_h \in \mathbf{W}_{h0}^D, \quad (3.1b)$$

$$(\nabla \cdot \mathbf{u}_{\delta t h}, q_h) + (q_h, \nabla \cdot \mathbf{z}_h^n) + J(p_{\delta t h}, q_h) = (g^n, q_h) \quad \forall q_h \in Q_h. \quad (3.1c)$$

We also choose the following initial conditions

$$a(\mathbf{u}_h^0, \mathbf{v}) = a(\mathbf{u}^0, \mathbf{v}) \quad \forall \mathbf{v}_h \in \mathbf{W}_{h0}^E, \quad (3.2a)$$

$$(p_h^0, q_h) = (p^0, q_h) \quad \forall q_h \in Q_h. \quad (3.2b)$$

The stabilization term is given by, see [9],

$$J(p, q) = \delta \sum_K \int_{\partial K \setminus \partial \Omega} h_{\partial K} [p][q] \, ds.$$

Here δ is a penalty parameter that is independent of h and Δt . We see in the numerical results, section 5 that the convergence is not sensitive to δ . The set of all elements is denoted by K , $h_{\partial K}$ denotes the size of an element edge in 2D or face in 3D, and $[\cdot]$ is the jump across an edge. As an example consider $[p_h]$, the jump operator on the piecewise constant pressure. The jump in pressure $[p_h]$ across an element or face E adjoining elements T and S is defined as

$$[p_h] := (p_h|_T - p_h|_S) \cdot \mathbf{n}_{E,T} = (p_h|_S - p_h|_T) \cdot \mathbf{n}_{E,S}.$$

Here $\mathbf{n}_{E,T}$ is the outward normal from element T , with respect to edge E , $\mathbf{n}_{E,S}$ is the corresponding inward facing normal, and $p_h|_T$ and $p_h|_S$ denote the pressure in element T and S , respectively. The stabilization term also gives rise to the norm $\|q\|_{J,\Omega} = J(q, q)^{1/2}$. Throughout this work, we will let C denote a generic positive constant, whose value may change from instance to instance, but is independent of any mesh parameters. We now have the following bound for the stabilization term

$$J(q_h, q_h) \leq \|q_h\|_{J,\Omega} \|q_h\|_{J,\Omega} \leq \left(C \|q_h\|_{0,\Omega}^2 + hC \|q_h\|_{1,\Omega} \|q_h\|_{0,\Omega} \right) \leq \|q_h\|_{0,\Omega}^2. \quad (3.3)$$

The first inequality above comes from an application of the Cauchy-Schwarz inequality, the second step is possible due to the the following trace inequality from lemma 3.1 in [37], which can be written as

$$\|\mathbf{v} \cdot \mathbf{n}\|_{0,\partial K}^2 \leq C \|\mathbf{v}\|_{0,K} (h^{-1} \|\mathbf{v}\|_{0,K} + \|\mathbf{v}\|_{1,K}), \quad (3.4)$$

and in the final step we have used the inverse estimate $\|v\|_{1,\Omega} \leq \frac{C}{h} \|v\|_{0,\Omega}$.

3.1 Existence and uniqueness of the fully-discrete model at a time step

Combining the fully discrete balance equations (3.1a), (3.1b) and (3.1c), and multiplying (3.1b) and (3.1c) by Δt we get the following

$$B_h^n[(\mathbf{u}_h, \mathbf{z}_h, p_h), (\mathbf{v}_h, \mathbf{w}_h, q_h)] = (\mathbf{f}^n, \mathbf{v}_h) + (\mathbf{t}_N, \mathbf{v}_h)_{\Gamma_t} + \Delta t(\mathbf{b}^n, \mathbf{w}_h) - \Delta t(p_D, \mathbf{w}_h \cdot \mathbf{n})_{\Gamma_p} + \Delta t(g^n, q_h) + (\nabla \cdot \mathbf{u}_h^{n-1}, q_h) + J(p_h^{n-1}, q_h) \quad \forall (\mathbf{v}_h, \mathbf{w}_h, q_h) \in \mathcal{W}_h^X, \quad (3.5)$$

where

$$B_h^n[(\mathbf{u}_h, \mathbf{z}_h, p_h), (\mathbf{v}_h, \mathbf{w}_h, q_h)] = a(\mathbf{u}_h^n, \mathbf{v}_h) + \Delta t(\boldsymbol{\kappa}^{-1} \mathbf{z}_h^n, \mathbf{w}_h) - (p_h^n, \nabla \cdot \mathbf{v}_h) - \Delta t(p_h^n, \nabla \cdot \mathbf{w}_h) + (\nabla \cdot \mathbf{u}_h^n, q_h) + \Delta t(\nabla \cdot \mathbf{z}_h^n, q_h) + J(p_h^n, q_h). \quad (3.6)$$

We also define the following triple-norm:

$$\|(\mathbf{u}_h^n, \mathbf{z}_h^n, p_h^n)\|_{\mathcal{W}_h^X} = \|\mathbf{u}_h^n\|_{1,\Omega} + \Delta t \|\nabla \cdot \mathbf{z}_h^n\|_{0,\Omega} + \Delta t^{1/2} \|\mathbf{z}_h^n\|_{0,\Omega} + \|p_h^n\|_{0,\Omega} + \|p_h^n\|_{J,\Omega}, \quad (3.7)$$

and for the test functions the triple-norm:

$$\|(\mathbf{v}_h, \mathbf{w}_h, q_h)\|_{\mathcal{V}_h^X} = \|\mathbf{v}_h\|_{1,\Omega} + \|\nabla \cdot \mathbf{w}_h\|_{0,\Omega} + \Delta t^{1/2} \|\mathbf{w}_h\|_{0,\Omega} + \|q_h\|_{0,\Omega} + \|q_h\|_{J,\Omega}. \quad (3.8)$$

Note that these triple-norms satisfies the required continuity property

$$|B_h^n[(\mathbf{u}_h, \mathbf{z}_h, p_h), (\mathbf{v}_h, \mathbf{w}_h, q_h)]| \leq C \|(\mathbf{u}_h^n, \mathbf{z}_h^n, p_h^n)\|_{\mathcal{W}_h^X} \|(\mathbf{v}_h, \mathbf{w}_h, q_h)\|_{\mathcal{V}_h^X}.$$

We will now apply Babuska's theory [3] to show well-posedness (existence and uniqueness) of this discretized system at a particular time step. This requires us to prove an inf-sup type result (Theorem 3.1) for the combined bilinear form (3.6). This will ensure that the resulting linear system from the discretization is full rank and has a solution.

Theorem 3.1. *Let $\gamma > 0$ be a constant independent of any mesh parameters. Then the finite element formulation (3.1) satisfies the following inf-sup condition*

$$\gamma \|(\mathbf{u}_h^n, \mathbf{z}_h^n, p_h^n)\|_{\mathcal{W}_h^X} \leq \sup_{(\mathbf{v}_h, \mathbf{w}_h, q_h) \in \mathcal{V}_h^X} \frac{B_h^n[(\mathbf{u}_h, \mathbf{z}_h, p_h), (\mathbf{v}_h, \mathbf{w}_h, q_h)]}{\|(\mathbf{v}_h, \mathbf{w}_h, q_h)\|_{\mathcal{V}_h^X}} \quad \forall (\mathbf{u}_h, \mathbf{z}_h, p_h) \in \mathcal{W}_h^X. \quad (3.9)$$

The following proof follows ideas presented by Burman and Hansbo [9].

Proof. Step 1, bounding $\|\mathbf{u}_h^n\|_{1,\Omega}$, $\Delta t^{1/2} \|\mathbf{z}_h^n\|_{0,\Omega}$, and $\|p_h^n\|_{J,\Omega}$.

Choose $(\mathbf{v}_h, \mathbf{w}_h, q_h) = (\mathbf{u}_h^n, \mathbf{z}_h^n, p_h^n)$, then using (2.2) and (2.3), we obtain,

$$B_h^n[(\mathbf{u}_h, \mathbf{z}_h, p_h), (\mathbf{u}_h, \mathbf{z}_h, p_h)] = a(\mathbf{u}_h^n, \mathbf{u}_h^n) + \Delta t(\boldsymbol{\kappa}^{-1} \mathbf{z}_h^n, \mathbf{z}_h^n) + J(p_h^n, p_h^n) \geq C_K \|\mathbf{u}_h^n\|_{1,\Omega}^2 + \lambda_{max}^{-1} \Delta t \|\mathbf{z}_h^n\|_{0,\Omega}^2 + \|p_h^n\|_{J,\Omega}^2. \quad (3.10)$$

Step 2, bounding $\|p_h^n\|_{0,\Omega}$.

Due to the surjectivity of the divergence operator there exists a function $\mathbf{v}_p \in [H_0^1]^d$ such that $\nabla \cdot \mathbf{v}_p = p_h^n$ and $\|\mathbf{v}_p\|_{1,\Omega} \leq c\|p_h^n\|_{0,\Omega}$, with $p_h^n \in Q_h$. Let $\pi_h \mathbf{v}_p$ denote the projection of $\mathbf{v}_p \in [H_0^1]^d$ onto \mathbf{W}_{h0}^E . This projection is known as the Scott-Zhang projection, see section 4.8 in [8] for details. We assume that the projection is stable such that

$$\|\pi_h \mathbf{v}_p\|_{1,\Omega} \leq \hat{c}\|p_h^n\|_{0,\Omega}, \quad (3.11)$$

which also gives

$$\|\pi_h \mathbf{v}_p\|_{0,\Omega} \leq \hat{c}\|p_h^n\|_{0,\Omega}. \quad (3.12)$$

Choose $(\mathbf{v}_h, \mathbf{w}_h, q_h) = (\pi_h \mathbf{v}_p, 0, 0)$ and add $0 = \|p_h^n\|_{0,\Omega}^2 - (p_h^n, \nabla \cdot \mathbf{v}_p)$ to obtain

$$B_h^n[(\mathbf{u}_h, \mathbf{z}_h, p_h), (\pi_h \mathbf{v}_p, 0, 0)] = a(\mathbf{u}_h^n, \pi_h \mathbf{v}_p) + \|p_h^n\|_{0,\Omega}^2 + (p_h^n, \nabla \cdot (\mathbf{v}_p - \pi_h \mathbf{v}_p)). \quad (3.13)$$

Focusing on the third term in (3.13) only, we apply the divergence theorem and split the integral over local elements to get

$$(p_h^n, \nabla \cdot (\mathbf{v}_p - \pi_h \mathbf{v}_p)) = \sum_K \int_{\partial k} p_h^n \cdot (\mathbf{v}_p - \pi_h \mathbf{v}_p) \cdot \mathbf{n} \, ds = \sum_K \frac{1}{2} \int_{\partial k} [p_h^n] \cdot (\mathbf{v}_p - \pi_h \mathbf{v}_p) \cdot \mathbf{n} \, ds.$$

We thus have

$$B_h^n[(\mathbf{u}_h, \mathbf{z}_h, p_h), (\pi_h \mathbf{v}_p, 0, 0)] - \|p_h^n\|_{0,\Omega}^2 = a(\mathbf{u}_h^n, \pi_h \mathbf{v}_p) + \sum_K \frac{1}{2} \int_{\partial k} [p_h^n] \cdot (\mathbf{v}_p - \pi_h \mathbf{v}_p) \cdot \mathbf{n} \, ds.$$

Now first applying the Cauchy-Schwarz inequality and (2.1) on the right hand side we get

$$\begin{aligned} B_h^n[(\mathbf{u}_h, \mathbf{z}_h, p_h), (\pi_h \mathbf{v}_p, 0, 0)] - \|p_h^n\|_{0,\Omega}^2 &\leq C_c \|\mathbf{u}_h^n\|_{1,\Omega} \|\pi_h \mathbf{v}_p\|_{1,\Omega} \\ &+ \sum_K \frac{1}{2} \left(\int_{\partial k} \left(h^{1/2} [p_h^n] \right)^2 \, ds \right)^{1/2} \cdot \left(\int_{\partial k} \left(h^{-1/2} (\mathbf{v}_p - \pi_h \mathbf{v}_p) \cdot \mathbf{n} \right)^2 \, ds \right)^{1/2}. \end{aligned}$$

Now apply Young's inequality and the bound of the projection (3.11), to obtain

$$\begin{aligned} B_h^n[(\mathbf{u}_h, \mathbf{z}_h, p_h), (\pi_h \mathbf{v}_p, 0, 0)] - \|p_h^n\|_{0,\Omega}^2 &\leq \frac{C_c^2}{2\alpha} \|\mathbf{u}_h^n\|_{1,\Omega}^2 + \frac{\alpha \hat{c}}{2} \|p_h^n\|_{0,\Omega}^2 \\ &+ \frac{1}{4\alpha} J(p_h^n, p_h^n) + \frac{\alpha}{4} \sum_K \int_{\partial k} h^{-1} |(\mathbf{v}_p - \pi_h \mathbf{v}_p) \cdot \mathbf{n}|^2 \, ds. \end{aligned}$$

Hence,

$$\begin{aligned} B_h^n[(\mathbf{u}_h, \mathbf{z}_h, p_h), (\pi_h \mathbf{v}_p, 0, 0)] &\geq -\frac{C_c^2}{2\alpha} \|\mathbf{u}_h^n\|_{1,\Omega}^2 + \left(1 - \frac{\alpha \hat{c}}{2}\right) \|p_h^n\|_{0,\Omega}^2 \\ &- \frac{1}{4\alpha} J(p_h^n, p_h^n) - \frac{\alpha}{4} \sum_K \int_{\partial k} h^{-1} |(\mathbf{v}_p - \pi_h \mathbf{v}_p) \cdot \mathbf{n}|^2 \, ds. \end{aligned}$$

Recall the trace inequality from lemma 3.1 in [37], which can be written as

$$\|\mathbf{v} \cdot \mathbf{n}\|_{0,\partial K}^2 \leq C \|\mathbf{v}\|_{0,K} (h^{-1} \|\mathbf{v}\|_{0,K} + \|\mathbf{v}\|_{1,K}). \quad (3.14)$$

Substituting $\mathbf{v} = (\mathbf{v}_p - \pi_h \mathbf{v}_p)$ in (3.14) and noting that $\|\mathbf{v}_p - \pi_h \mathbf{v}_p\|_{0,K} \leq Ch\|\mathbf{v}_p\|_{1,K}$ we arrive at

$$\|(\mathbf{v}_p - \pi_h \mathbf{v}_p) \cdot \mathbf{n}\|_{0,\partial K}^2 \leq Ch\|\mathbf{v}_p\|_{1,K}^2.$$

Taking into account $\|\mathbf{v}_p\|_{1,\Omega} \leq c\|p_h^n\|_{0,\Omega}$, we may write

$$\sum_K \int_{\partial K} h^{-1} |(\mathbf{v}_p - \pi_h \mathbf{v}_p) \cdot \mathbf{n}|^2 ds \leq c_t \|p_h^n\|_{0,\Omega}^2,$$

which leads to

$$B_h^n[(\mathbf{u}_h, \mathbf{z}_h, p_h), (\pi_h \mathbf{v}_p, 0, 0)] \geq -\frac{C_c^2}{2\alpha} \|\mathbf{u}_h^n\|_{1,\Omega}^2 + \left(1 - \left(\hat{c} + \frac{c_t}{2}\right) \frac{\alpha}{2}\right) \|p_h^n\|_{0,\Omega}^2 - \frac{1}{4\alpha} \|p_h^n\|_{J,\Omega}^2. \quad (3.15)$$

Step 3, bounding $\Delta t \|\nabla \cdot \mathbf{z}_h^n\|_{0,\Omega}$.

Choosing $(\mathbf{v}_h, \mathbf{w}_h, q_h) = (0, 0, \Delta t \nabla \cdot \mathbf{z}_h^n)$ yields

$$B_h^n[(\mathbf{u}_h, \mathbf{z}_h, p_h), (0, 0, \Delta t \nabla \cdot \mathbf{z}_h^n)] = (\nabla \cdot \mathbf{u}_h^n, \Delta t \nabla \cdot \mathbf{z}_h^n) + \Delta t^2 \|\nabla \cdot \mathbf{z}_h^n\|_{0,\Omega}^2 + J(p_h^n, \Delta t \nabla \cdot \mathbf{z}_h^n).$$

We bound the first term using the Cauchy-Schwarz inequality followed by Young's inequality such that

$$(\nabla \cdot \mathbf{u}_h^n, \Delta t \nabla \cdot \mathbf{z}_h^n) \leq \frac{C_p}{2\alpha} \|\mathbf{u}_h^n\|_{1,\Omega}^2 + \frac{\alpha \Delta t^2}{2} \|\nabla \cdot \mathbf{z}_h^n\|_{0,\Omega}^2.$$

We can also bound the third term as before using the Cauchy-Schwarz inequality followed by Young's inequality such that

$$\begin{aligned} J(p_h^n, \Delta t \nabla \cdot \mathbf{z}_h^n) &\leq \frac{1}{2\alpha} J(p_h^n, p_h^n) + \frac{\alpha \Delta t^2}{2} J(\nabla \cdot \mathbf{z}_h^n, \nabla \cdot \mathbf{z}_h^n) \leq \frac{1}{2\alpha} J(p_h^n, p_h^n) + \alpha C \Delta t^2 \sum_K \int_{\partial K} |h^{1/2} \nabla \cdot \mathbf{z}_h^n|^2 ds \\ &\leq \frac{1}{2\alpha} J(p_h^n, p_h^n) + \alpha c_z \Delta t^2 \|\nabla \cdot \mathbf{z}_h^n\|_{0,\Omega}^2. \end{aligned} \quad (3.16)$$

Here we have used a scaling argument which relates line and surface integrals and assumes that $\nabla \cdot \mathbf{z}_h^n$ is element-wise constant. The scaling argument, also used in [9], is that $C \|h^{1/2} \nabla \cdot \mathbf{z}_h^n\|_{0,\partial K} \leq c_z \|\nabla \cdot \mathbf{z}_h^n\|_{0,K}$. This yields

$$B_h^n[(\mathbf{u}_h, \mathbf{z}_h, p_h), (0, 0, \Delta t \nabla \cdot \mathbf{z}_h^n)] \geq \left(1 - \alpha c_z - \frac{\alpha}{2}\right) \Delta t^2 \|\nabla \cdot \mathbf{z}_h^n\|_{0,\Omega}^2 - \frac{1}{2\alpha} \|p_h^n\|_{J,\Omega}^2 - \frac{C_p}{2\alpha} \|\mathbf{u}_h^n\|_{1,\Omega}^2. \quad (3.17)$$

Combining all the steps. Finally we can combine (3.10), (3.15) and (3.17) to get control over all the norms by choosing $(\mathbf{v}_h, \mathbf{w}_h, q_h) = (\beta \mathbf{u}_h^n + \pi_h \mathbf{v}_p, \beta \mathbf{z}_h^n, \beta p_h^n + \Delta t \nabla \cdot \mathbf{z}_h^n)$, which yields

$$\begin{aligned} B_h^n[(\mathbf{u}_h, \mathbf{z}_h, p_h), (\beta \mathbf{u}_h^n + \pi_h \mathbf{v}_p, \beta \mathbf{z}_h^n, \beta p_h^n + \Delta t \nabla \cdot \mathbf{z}_h^n)] &\geq \\ &(\beta C_K - \frac{C_c^2 + C_p}{2\alpha}) \|\mathbf{u}_h^n\|_{1,\Omega}^2 + \beta \lambda_{max}^{-1} \Delta t \|\mathbf{z}_h^n\|_{0,\Omega}^2 + \left(1 - \alpha c_z - \frac{\alpha}{2}\right) \Delta t^2 \|\nabla \cdot \mathbf{z}_h^n\|_{0,\Omega}^2 \\ &\quad + \left(1 - \left(\hat{c} + \frac{c_t}{2}\right) \frac{\alpha}{2}\right) \|p_h^n\|_{0,\Omega}^2 + \left(\beta - \frac{3}{4\alpha}\right) \|p_h^n\|_{J,\Omega}^2, \end{aligned}$$

where we can choose

$$\beta \geq \max \left[\frac{C_c^2 + C_p}{2\alpha C_k} + \frac{1 - \bar{C}\alpha}{C_k}, \lambda_{max} (1 - \bar{C}\alpha), \frac{3}{4\alpha} + 1 - \bar{C}\alpha \right],$$

with $\bar{C} = \max \left[\frac{\hat{c}}{2} + \frac{c_t}{4}, c_z - \frac{1}{2} \right]$. This yields

$$B_h^n[(\mathbf{u}_h, \mathbf{z}_h, p_h), (\beta \mathbf{u}_h^n + \pi_h \mathbf{v}_p, \beta \mathbf{z}_h^n, \beta p_h^n + \nabla \cdot \mathbf{z}_h^n)] \geq (1 - \bar{C}\alpha) \|(\mathbf{u}_h^n, \mathbf{z}_h^n, p_h^n)\|_{\mathcal{W}_h^X}^2.$$

To complete the proof we need to take α sufficiently small and show that there exists a constant C such that $\|(\mathbf{u}_h^n, \mathbf{z}_h^n, p_h^n)\|_{\mathcal{W}_h^X} \geq C \|(\mathbf{v}_h, \mathbf{w}_h, q_h)\|_{\mathcal{V}_h^X}$, with $(\mathbf{v}_h, \mathbf{w}_h, q_h) = (\beta \mathbf{u}_h^n + \pi_h \mathbf{v}_p, \beta \mathbf{z}_h^n, \beta p_h^n + \Delta t \nabla \cdot \mathbf{z}_h^n)$. Using the definition of the previously defined norms (3.7) and (3.8), we have

$$\begin{aligned} \|(\beta \mathbf{u}_h^n + \pi_h \mathbf{v}_p, \beta \mathbf{z}_h^n, \beta p_h^n + \Delta t \nabla \cdot \mathbf{z}_h^n)\|_{\mathcal{W}_h^X} &= \beta \|\mathbf{u}_h^n\|_{1,\Omega} + \|\pi_h \mathbf{v}_p\|_{1,\Omega} + \Delta t \|\nabla \cdot \mathbf{z}_h^n\|_{0,\Omega} \\ &\quad + \beta \Delta t^{1/2} \|\mathbf{z}_h^n\|_{0,\Omega} + \beta \|p_h^n\|_{0,\Omega} + \beta \|p_h^n\|_{J,\Omega} \\ &\leq C \|(\mathbf{u}_h^n, \mathbf{z}_h^n, p_h^n)\|_{\mathcal{W}_h^X}. \end{aligned}$$

This completes the proof. \square

3.2 Energy estimate of the fully-discrete model

In this section we present some lemmas that build towards an energy estimate for the fully-discrete model. Combining (3.1a), (3.1b) and (3.1c), multiplying by Δt , summing, and assuming $p_D = 0$ on Γ_p and $\mathbf{t}_N = 0$ on Γ_t we get the following

$$\begin{aligned} \sum_{n=1}^N \Delta t B_{\delta t, h}^n[(\mathbf{u}_h, \mathbf{z}_h, p_h), (\mathbf{v}_h, \mathbf{w}_h, q_h)] &= \sum_{n=1}^N \Delta t (\mathbf{f}^n, \mathbf{v}_h) + \sum_{n=1}^N \Delta t (\mathbf{b}^n, \mathbf{w}_h) \\ &\quad + \sum_{n=1}^N \Delta t (g^n, q_h) \quad \forall (\mathbf{v}_h, \mathbf{w}_h, q_h) \in \mathcal{W}_h^X, \end{aligned} \quad (3.18)$$

where

$$\begin{aligned} B_{\delta t, h}^n[(\mathbf{u}_h, \mathbf{z}_h, p_h), (\mathbf{v}_h, \mathbf{w}_h, q_h)] &= a(\mathbf{u}_h^n, \mathbf{v}_h) + (\boldsymbol{\kappa}^{-1} \mathbf{z}_h^n, \mathbf{w}_h) - (p_h^n, \nabla \cdot \mathbf{v}_h) - (p_h^n, \nabla \cdot \mathbf{w}_h) \\ &\quad + (\nabla \cdot \mathbf{u}_{\delta t, h}^n, q_h) + (\nabla \cdot \mathbf{z}_h^n, q_h) + J(p_{\delta t, h}^n, q_h). \end{aligned} \quad (3.19)$$

Lemma 3.2. *Let $\pi_h \mathbf{v}_p$ be the projection of some of $\mathbf{v}_p \in [H_0^1]^d$ onto \mathbf{W}_{h0}^E . Then for all $(\mathbf{u}_h^n, \mathbf{z}_h^n, p_h^n) \in (\mathbf{W}_h^E \times \mathbf{W}_h^D \times Q_h)$ the combined bilinear form (3.19) satisfies*

$$\begin{aligned} \sum_{n=0}^N \Delta t B_{\delta t, h}^n[(\mathbf{u}_h, \mathbf{z}_h, p_h), (\mathbf{u}_{\delta t, h}^n + \pi_h \mathbf{v}_p, \mathbf{z}_h^n, p_h^n)] &\geq \\ &C \left(\|\mathbf{u}_h^N\|_{1,\Omega}^2 + \|p_h^N\|_{J,\Omega}^2 + \|\mathbf{z}_h\|_{l^2(L_2)}^2 + \|p_h\|_{l^2(L_2)}^2 \right). \end{aligned}$$

Proof. Choosing $\mathbf{v}_h = \mathbf{u}_{\delta t_h}^n + \pi_h \mathbf{v}_p$, $\mathbf{w}_h = \mathbf{z}_h^n$, $q_h = p_h^n$, with $\nabla \cdot \mathbf{v}_p = p_h^n$ in (3.19) we get

$$\begin{aligned} \sum_{n=1}^N \Delta t B_{\delta t, h}^n[(\mathbf{u}_h, \mathbf{z}_h, p_h), (\mathbf{u}_{\delta t_h}^n + \pi_h \mathbf{v}_p, \mathbf{z}_h^n, p_h^n)] &= \sum_{n=1}^N \Delta t a(\mathbf{u}_h^n, \mathbf{u}_{\delta t_h}^n) + \sum_{n=1}^N \Delta t a(\mathbf{u}_h^n, \pi_h \mathbf{v}_p) \\ &\quad - \sum_{n=1}^N \Delta t (p_h^n, \nabla \cdot \pi_h \mathbf{v}_p) + \sum_{n=1}^N \Delta t \boldsymbol{\kappa}^{-1}(\mathbf{z}_h^n, \mathbf{z}_h^n) + \sum_{n=1}^N \Delta t J(p_{\delta t_h}^n, p_h^n). \end{aligned} \quad (3.20)$$

We now bound each of the above terms on the right hand side of (3.20) individually before combining the results.

$$\begin{aligned} \sum_{n=1}^N \Delta t a(\mathbf{u}_h^n, \mathbf{u}_{\delta t_h}^n) &= \sum_{n=1}^N \Delta t \left(\frac{1}{\Delta t} \|\mathbf{u}_h^n\|_{a, \Omega}^2 - \frac{1}{\Delta t} a(\mathbf{u}_h^n, \mathbf{u}_h^{n-1}) \right) \\ &\geq \frac{C_k}{2} \|\mathbf{u}_h^N\|_{1, \Omega}^2 - \frac{C_c}{2} \|\mathbf{u}_h^0\|_{1, \Omega}^2, \end{aligned} \quad (3.21)$$

where we have used (2.2) in the last step. Using (3.15) we have

$$\begin{aligned} \sum_{n=1}^N \Delta t a(\mathbf{u}_h^n, \pi_h \mathbf{v}_p) - \sum_{n=1}^N \Delta t (p_h^n, \nabla \cdot \pi_h \mathbf{v}_p) &\geq -\frac{C_c}{2\alpha} \|\mathbf{u}_h\|_{l^2(H^1)}^2 + \left(1 - \left(\hat{c} + \frac{c_t}{2}\right) \frac{\alpha}{2}\right) \|p_h\|_{l^2(L_2)}^2 \\ &\quad - \frac{1}{4\alpha} \|p_h\|_{l^2(J)}^2. \end{aligned} \quad (3.22)$$

Using (2.3),

$$\sum_{n=1}^N \Delta t (\boldsymbol{\kappa}^{-1}(\mathbf{z}_h^n, \mathbf{z}_h^n)) \geq \lambda_{max}^{-1} \|\mathbf{z}_h\|_{l^2(L_2)}^2. \quad (3.23)$$

The intermediate steps for the next bound have been omitted because they are very similar to (3.21). Thus

$$\sum_{n=1}^N \Delta t J(p_{\delta t_h}^n, p_h^n) \geq \frac{1}{2} \|p_h^N\|_{J, \Omega}^2. \quad (3.24)$$

We can now combine these intermediate results (3.21), (3.22), (3.23) and (3.24) to obtain from (3.20)

$$\begin{aligned} \sum_{n=0}^N \Delta t B_{\delta t, h}^n[(\mathbf{u}_h, \mathbf{z}_h, p_h), (\mathbf{u}_{\delta t_h}^n + \pi_h \mathbf{v}_p, \mathbf{z}_h^n, p_h^n)] &+ \frac{C_c}{2} \|\mathbf{u}_h^0\|_{1, \Omega}^2 + \frac{C_c}{2\alpha} \|\mathbf{u}_h\|_{l^2(H^1)}^2 + \frac{1}{4\alpha} \|p_h\|_{l^2(J)}^2 \\ &\geq \frac{C_k}{2} \|\mathbf{u}_h^N\|_{1, \Omega}^2 + \frac{1}{2} \|p_h^N\|_{J, \Omega}^2 + \lambda_{max}^{-1} \|\mathbf{z}_h\|_{l^2(L_2)}^2 + (1 - C\alpha) \|p_h\|_{l^2(L_2)}^2. \end{aligned} \quad (3.25)$$

Finally choosing α small, using (2.1) and (2.6), and applying a discrete version of Gronwall's lemma (see [34]) completes the proof. \square

Lemma 3.3. *The combined finite element formulation (3.18) satisfies*

$$\|\mathbf{u}_h^N\|_{1,\Omega}^2 + \|p_h^N\|_{J,\Omega}^2 + \|\mathbf{z}_h\|_{l^2(L_2)}^2 + \|p_h\|_{l^2(L_2)}^2 \leq C.$$

Proof. Choosing $\mathbf{v}_h = \mathbf{u}_{\delta t_h}^n + \pi_h \mathbf{v}_p$, $\mathbf{w}_h = \mathbf{z}_h^n$, $q_h = p_h^n$, with $\nabla \cdot \mathbf{v}_p = p_h^n$ in (3.18), multiplying by Δt , and summing yields

$$\begin{aligned} \sum_{n=1}^N \Delta t B_h[(\mathbf{u}_h^n, \mathbf{z}_h^n, p_h^n), (\mathbf{u}_{\delta t_h}^n + \pi_h \mathbf{v}_p, \mathbf{z}_h^n, p_h^n)] &= \sum_{n=1}^N \Delta t (\mathbf{f}^n, \mathbf{u}_{\delta t_h}^n + \pi_h \mathbf{v}_p) \\ &+ \sum_{n=1}^N \Delta t (\mathbf{b}^n, \mathbf{z}_h^n) + \sum_{n=1}^N \Delta t (g^n, p_h^n). \end{aligned}$$

Let us note that,

$$\sum_{n=1}^N \Delta t (\mathbf{f}^n, \mathbf{u}_{\delta t_h}^n) = \sum_{n=1}^N (\mathbf{f}^n, \mathbf{u}_h^n - \mathbf{u}_h^{n-1}) = (\mathbf{f}^N, \mathbf{u}_h^N) - (\mathbf{f}^1, \mathbf{u}_h^0) - \sum_{n=1}^{N-1} (\mathbf{f}^{n+1} - \mathbf{f}^n, \mathbf{u}_h^n), \quad (3.26)$$

and further that

$$\begin{aligned} - \sum_{n=1}^{N-1} (\mathbf{f}^{n+1} - \mathbf{f}^n, \mathbf{u}_h^n) &\leq C \sum_{n=1}^{N-1} \|\mathbf{f}^{n+1} - \mathbf{f}^n\|_{0,\Omega} \|\mathbf{u}_h^n\|_{0,\Omega} \leq C \sum_{n=1}^{N-1} \left\{ \int_{t_n}^{t_{n+1}} \|\dot{\mathbf{f}}\|_{0,\Omega} \right\}^{1/2} \|\mathbf{u}_h^n\|_{1,\Omega} \\ &\leq C \left(\frac{1}{2\alpha} \|\dot{\mathbf{f}}\|_{L^2(L_2)}^2 + \frac{\alpha}{2} \|\mathbf{u}_h\|_{l^2(L_2)}^2 \right). \end{aligned}$$

Now using the above, lemma 3.2, the Cauchy-Schwarz and Young's inequalities, and noting (3.12), we arrive at

$$\begin{aligned} &(1 - \frac{\alpha}{2}) \|\mathbf{u}_h^N\|_{1,\Omega}^2 + \|p_h^N\|_{J,\Omega}^2 + (1 - \frac{\alpha}{2}) \|\mathbf{z}_h\|_{l^2(L_2)}^2 + (1 - \frac{\alpha}{2}) \|p_h\|_{l^2(L_2)}^2 \\ &\leq \frac{C_k}{2\alpha} \|\mathbf{u}_h\|_{l^2(H^1)}^2 + \frac{1}{4\alpha} \|p_h\|_{l^2(J)}^2 + \frac{1}{\alpha} \|\mathbf{f}^N\|_{0,\Omega}^2 + \frac{C}{2\alpha} \|\dot{\mathbf{f}}\|_{L^2(L_2)}^2 + \frac{C\alpha}{2} \|\mathbf{u}_h\|_{l^2(L_2)}^2 + \frac{\alpha}{2} \|\mathbf{u}_h^0\|_{0,\Omega}^2 \\ &\quad + \frac{1}{2\alpha} \|\mathbf{f}\|_{l^2(L_2)}^2 + \frac{\alpha \hat{c}}{2} \|\mathbf{u}_h\|_{l^2(L_2)}^2 + \frac{1}{2\alpha} \|\mathbf{b}\|_{l^2(L_2)}^2 + \frac{1}{2\alpha} \|g\|_{l^2(L_2)}^2. \end{aligned}$$

Finally choosing α small, applying a discrete version of Gronwall's lemma, using (2.5a), (2.5b), (2.5c) and (2.6), we arrive at the desired result. \square

To get a bound for the fluid flux in its natural *Hdiv* norm we now define another combined bilinear form B_h^* . We first show how we derive B_h^* from the weak form (3.18), for which we know that a solution $(\mathbf{u}_h, \mathbf{z}_h, p_h)$ exists for test functions $(\mathbf{v}_h, \mathbf{w}_h, q_h) \in \mathcal{V}_h^X$. Choosing test functions $(\frac{\mathbf{v}_h}{\Delta t}, \frac{\mathbf{w}_h}{\Delta t}, 0)$ in (3.18) we have

$$\begin{aligned} \sum_{n=1}^N B_{\delta t,h}^n[(\mathbf{u}_h, \mathbf{z}_h, p_h), (\frac{\mathbf{v}_h}{\Delta t}, \frac{\mathbf{w}_h}{\Delta t}, 0)] &= \sum_{n=1}^N a(\mathbf{u}_h^n, \mathbf{v}_h) + \sum_{n=1}^N (\boldsymbol{\kappa}^{-1} \mathbf{z}_h^n, \mathbf{w}_h) \\ &\quad - \sum_{n=1}^N (p_h^n, \nabla \cdot \mathbf{v}_h) - \sum_{n=1}^N (p_h^n, \nabla \cdot \mathbf{w}_h) \\ &= \sum_{n=1}^N (\mathbf{f}^n, \mathbf{v}_h) + \sum_{n=1}^N (\mathbf{b}^n, \mathbf{w}_h) \quad \forall (\mathbf{v}_h, \mathbf{w}_h, q_h) \in \mathcal{V}_h^X. \quad (3.27) \end{aligned}$$

Choosing $(\frac{\mathbf{v}_h}{\Delta t}, \frac{\mathbf{w}_h}{\Delta t}, 0)$ in (3.18), summing from 0 to $N - 1$ and introducing an initial condition for the fluid flux $\mathbf{z}_h^0 = \mathbf{z}^0$, we have

$$\begin{aligned}
\sum_{n=0}^{N-1} B_{\delta t, h}^n[(\mathbf{u}_h, \mathbf{z}_h, p_h), (\frac{\mathbf{v}_h}{\Delta t}, \frac{\mathbf{w}_h}{\Delta t}, 0)] &= \sum_{n=1}^N B_{\delta t, h}^{n-1}[(\mathbf{u}_h, \mathbf{z}_h, p_h), (\frac{\mathbf{v}_h}{\Delta t}, \frac{\mathbf{w}_h}{\Delta t}, 0)] \\
&= \sum_{n=1}^N a(\mathbf{u}_h^{n-1}, \mathbf{v}_h) + \sum_{n=1}^N (\boldsymbol{\kappa}^{-1} \mathbf{z}_h^{n-1}, \mathbf{w}_h) - \sum_{n=1}^N (p_h^{n-1}, \nabla \cdot \mathbf{v}_h) - \sum_{n=1}^N (p_h^{n-1}, \nabla \cdot \mathbf{w}_h) \\
&= \sum_{n=1}^N (\mathbf{f}^{n-1}, \mathbf{v}_h) + \sum_{n=1}^N (\mathbf{b}^{n-1}, \mathbf{w}_h) \quad \forall (\mathbf{v}_h, \mathbf{w}_h, q_h) \in \mathcal{V}_h^X. \quad (3.28)
\end{aligned}$$

Finally choosing test functions $(0, 0, q_h)$ in (3.18) we have

$$\begin{aligned}
\sum_{n=1}^N \Delta t B_{\delta t, h}^n[(\mathbf{u}_h, \mathbf{z}_h, p_h), (0, 0, q_h)] &= \sum_{n=1}^N \Delta t (\nabla \cdot \mathbf{u}_{\delta t h}^n, q_h) + \sum_{n=1}^N \Delta t (\nabla \cdot \mathbf{z}_h^n, q_h) + \sum_{n=1}^N \Delta t J(p_{\delta t h}^n, q_h) \\
&= \sum_{n=1}^N \Delta t (g^n, q_h) \quad \forall (\mathbf{v}_h, \mathbf{w}_h, q_h) \in \mathcal{V}_h^X. \quad (3.29)
\end{aligned}$$

Now adding (3.27) and (3.29) and subtracting (3.28) we get

$$\begin{aligned}
\sum_{n=1}^N \Delta t B_h^*[(\mathbf{u}_h, \mathbf{z}_h, p_h), (\mathbf{v}_h, \mathbf{w}_h, q_h)] &= \sum_{n=1}^N \Delta t (\mathbf{f}_{\delta t}^n, \mathbf{v}_h) + \sum_{n=1}^N \Delta t (\mathbf{b}_{\delta t}^n, \mathbf{w}_h) \\
&\quad + \sum_{n=1}^N \Delta t (g^n, q_h) \quad \forall (\mathbf{v}_h, \mathbf{w}_h, q_h) \in \mathcal{V}_h^X, \quad (3.30)
\end{aligned}$$

where

$$\begin{aligned}
B_h^*[(\mathbf{u}_h, \mathbf{z}_h, p_h), (\mathbf{v}_h, \mathbf{w}_h, q_h)] &= a(\mathbf{u}_{\delta t h}^n, \mathbf{v}_h) + (\boldsymbol{\kappa}^{-1} \mathbf{z}_{\delta t h}^n, \mathbf{w}_h) - (p_{\delta t h}^n, \nabla \cdot \mathbf{v}_h) - (p_{\delta t h}^n, \nabla \cdot \mathbf{w}_h) \\
&\quad + (\nabla \cdot \mathbf{u}_{\delta t h}^n, q_h) + (\nabla \cdot \mathbf{z}_h, q_h) + J(p_{\delta t h}^n, q_h). \quad (3.31)
\end{aligned}$$

Lemma 3.4. *Let $\beta > 0$ and $\pi_h \mathbf{v}_p$ be the projection of some of $\mathbf{v}_p \in [H_0^1]^d$ onto \mathbf{W}_{h0}^E . Then for all $(\mathbf{u}_h^n, \mathbf{z}_h^n, p_h^n) \in (\mathbf{W}_h^E \times \mathbf{W}_h^D \times Q_h)$ the combined bilinear form (3.31) satisfies*

$$\begin{aligned}
\sum_{n=1}^N \Delta t B_h^*[(\mathbf{u}_h, \mathbf{z}_h, p_h), (\beta \mathbf{u}_{\delta t h}^n + \pi_h \mathbf{v}_p, \beta \mathbf{z}_h^n, \beta p_{\delta t h}^n)] &\geq \\
C \left(\|\mathbf{u}_{\delta t h}\|_{l^2(H^1)}^2 + \|\mathbf{z}_h^N\|_{0, \Omega}^2 + \|p_{\delta t h}\|_{l^2(L_2)}^2 + \|p_{\delta t h}\|_{l^2(J)}^2 + \|\nabla \cdot \mathbf{z}_h\|_{l^2(L_2)}^2 \right).
\end{aligned}$$

Proof. Choosing $\mathbf{v}_h = \beta \mathbf{u}_{\delta t_h}^n + \pi_h \mathbf{v}_p$, $\mathbf{w}_h = \beta \mathbf{z}_h^n$, $q_h = \beta p_{\delta t_h}^n + \nabla \cdot \mathbf{z}_h^n$, with $\pi_h \mathbf{v}_p$ in (3.31) we get

$$\begin{aligned}
& \sum_{n=1}^N \Delta t B_h^*[(\mathbf{u}_h, \mathbf{z}_h, p_h), (\beta \mathbf{u}_{\delta t_h}^n + \pi_h \mathbf{v}_p, \beta \mathbf{z}_h^n, \beta p_{\delta t_h}^n)] \\
&= \sum_{n=1}^N \Delta t a(\mathbf{u}_{\delta t_h}^n, \beta \mathbf{u}_{\delta t_h}^n) + \sum_{n=1}^N \Delta t \kappa^{-1}(\mathbf{z}_{\delta t_h}^n, \beta \mathbf{z}_h^n) + \sum_{n=1}^N \Delta t (\nabla \cdot \mathbf{z}_h^n, \nabla \cdot \mathbf{z}_h^n) + \sum_{n=1}^N \Delta t (\mathbf{u}_{\delta t_h}^n, \nabla \cdot \mathbf{z}_h^n) \\
&+ \sum_{n=1}^N \Delta t J(p_{\delta t_h}^n, \nabla \cdot \mathbf{z}_h^n) + \sum_{n=1}^N \Delta t J(p_{\delta t_h}^n, \beta p_{\delta t_h}^n) + \sum_{n=1}^N \Delta t a(\mathbf{u}_{\delta t_h}^n, \pi_h \mathbf{v}_p) - \sum_{n=1}^N \Delta t (p_{\delta t_h}^n, \nabla \cdot \pi_h \mathbf{v}_p).
\end{aligned} \tag{3.32}$$

We now give some individual intermediate bounds for the above terms on the right hand side of (3.32) before combining the results.

$$\sum_{n=1}^N \Delta t a(\mathbf{u}_{\delta t_h}^n, \beta \mathbf{u}_{\delta t_h}^n) \geq \beta C_k \|\mathbf{u}_{\delta t_h}^n\|_{l^2(H^1)}^2, \tag{3.33}$$

where we have used (2.2). Next using (2.3) we have

$$\sum_{n=1}^N \Delta t \kappa^{-1}(\mathbf{z}_{\delta t_h}^n, \beta \mathbf{z}_h^n) \geq \frac{\beta \lambda_{max}^{-1}}{2} \|\mathbf{z}_h^N\|_{0,\Omega}^2 - \frac{\beta \lambda_{min}^{-1}}{2} \|\mathbf{z}_h^0\|_{0,\Omega}^2. \tag{3.34}$$

Using the Cauchy-Schwarz, Young's and the Poincaré inequalities we have

$$\sum_{n=1}^N \Delta t (\mathbf{u}_{\delta t_h}^n, \nabla \cdot \mathbf{z}_h^n) \leq \frac{C_p}{2\alpha} \|\mathbf{u}_{\delta t_h}\|_{l^2(H^1)}^2 + \frac{\alpha}{2} \|\nabla \cdot \mathbf{z}_h\|_{l^2(L_2)}^2. \tag{3.35}$$

Again using the Cauchy-Schwarz and Young's inequalities and (3.16) we have

$$\Delta t J(p_{\delta t_h}^n, \nabla \cdot \mathbf{z}_h^n) \leq \frac{1}{2\alpha} \|p_{\delta t_h}\|_{l^2(J)}^2 + \alpha c_z \|\nabla \cdot \mathbf{z}_h\|_{l^2(L_2)}^2. \tag{3.36}$$

Using workings very similar to step 2 in the proof of Theorem 3.1 we have

$$\begin{aligned}
\sum_{n=1}^N \Delta t a(\mathbf{u}_{\delta t_h}^n, \pi_h \mathbf{v}_p) - \sum_{n=1}^N \Delta t (p_{\delta t_h}^n, \nabla \cdot \pi_h \mathbf{v}_p) &\geq -\frac{C_c}{2\alpha} \|\mathbf{u}_{th}\|_{l^2(H^1)}^2 + (1 - C\alpha) \|p_{\delta t_h}\|_{l^2(L_2)}^2 \\
&\quad - \frac{1}{4\alpha} \|p_{\delta t_h}\|_{l^2(J)}^2.
\end{aligned} \tag{3.37}$$

We can now combine these intermediate results to obtain the following result

$$\begin{aligned}
\sum_{n=1}^N \Delta t B_h^*[(\mathbf{u}_h, \mathbf{z}_h, p_h), (\beta \mathbf{u}_{\delta t_h}^n + \pi_h \mathbf{v}_p, \beta \mathbf{z}_h^n, \beta p_{\delta t_h}^n)] &\geq \left(\beta C_k - \frac{C_p + C_c}{2\alpha} \right) \|\mathbf{u}_{\delta t_h}\|_{l^2(H^1)}^2 \\
&+ \frac{\beta \lambda_{max}^{-1}}{2} \|\mathbf{z}_h^N\|_{0,\Omega}^2 + \left(\beta - \frac{3}{4\alpha} \right) \|p_{\delta t_h}\|_{l^2(J)}^2 + (1 - \alpha(1 + c_z)) \|\nabla \cdot \mathbf{z}_h\|_{l^2(L_2)}^2 \\
&\quad - \frac{\beta \lambda_{min}^{-1}}{2} \|\mathbf{z}_h^0\|_{0,\Omega}^2 + (1 - C\alpha) \|p_{\delta t_h}\|_{l^2(L_2)}^2.
\end{aligned} \tag{3.38}$$

Finally choosing α small, $\beta \geq \max \left[\frac{C_p}{2C_k\alpha}, \frac{3}{4\alpha} \right]$, and using (2.6), completes the proof. \square

Also note that as an auxillary result, which we will use later for proving the a-priori error estimate that

$$\begin{aligned} \sum_{n=1}^N \Delta t B_h^*[(\mathbf{u}_h, \mathbf{z}_h, p_h), (\beta \mathbf{u}_{\delta t_h}^n, \beta \mathbf{z}_h^n, \beta p_{\delta t_h}^n)] &\geq \left(\beta C_k - \frac{C_p}{2\alpha} \right) \|\mathbf{u}_{\delta t_h}\|_{l^2(H^1)}^2 + \frac{\beta \lambda_{max}^{-1}}{2} \|\mathbf{z}_h^N\|_{0,\Omega}^2 \\ &+ \left(\beta - \frac{1}{2\alpha} \right) \|p_{\delta t_h}\|_{l^2(J)}^2 + (1 - \alpha(1 + c_z)) \|\nabla \cdot \mathbf{z}_h\|_{l^2(L_2)}^2. \end{aligned} \quad (3.39)$$

Lemma 3.5. *The combined finite element formulation (3.30) satisfies*

$$\|\nabla \cdot \mathbf{z}_h\|_{l^2(L_2)}^2 \leq C.$$

Proof. Choosing $\mathbf{v}_h = \beta \mathbf{u}_{\delta t_h}^n + \pi_h \mathbf{v}_p$, $\mathbf{w}_h = \beta \mathbf{z}_h^n$, $q_h = \beta p_{\delta t_h}^n + \nabla \cdot \mathbf{z}_h^n$ in (3.30), multiplying by Δt , and summing yields

$$\begin{aligned} \sum_{n=1}^N \Delta t B_h^*[(\mathbf{u}_h^n, \mathbf{z}_h^n, p_h^n), (\beta \mathbf{u}_{\delta t_h}^n + \pi_h \mathbf{v}_p, \mathbf{z}_h^n, \beta p_{\delta t_h}^n + \nabla \cdot \mathbf{z}_h^n)] &= \sum_{n=1}^N \Delta t (\mathbf{f}_{\delta t}^n, \mathbf{u}_{\delta t_h}^n) + \sum_{n=1}^N \Delta t (\mathbf{b}_{\delta t}^n, \beta \mathbf{z}_h^n) \\ &+ \sum_{n=1}^N \Delta t (g^n, \beta p_{\delta t_h}^n). \end{aligned}$$

Here β is a constant that is chosen to be the same as in lemma 3.4. Using lemma 3.4, the Cauchy-Schwarz and Young's inequalities, noting (3.3), along with some workings already presented in the proof of lemma 3.3 we arrive at

$$\begin{aligned} &\|\mathbf{u}_{\delta t_h}\|_{l^2(H^1)}^2 + (1 - C\alpha) \|p_{\delta t_h}\|_{l^2(L_2)}^2 + \|p_{\delta t_h}\|_{l^2(J)}^2 + \|\mathbf{z}_h^N\|_{0,\Omega}^2 + \|\nabla \cdot \mathbf{z}_h\|_{l^2(L_2)}^2 \\ &\leq C \left(\|\dot{\mathbf{f}}\|_{L^2(L_2)}^2 + \|\mathbf{u}_{\delta t_h}\|_{l^2(L_2)}^2 + \|\dot{\mathbf{b}}\|_{L^2(L_2)}^2 + \|\mathbf{z}_h\|_{l^2(L_2)}^2 + \frac{1}{\alpha} \|g\|_{L^2(L_2)}^2 \right). \end{aligned}$$

Finally applying a discrete version of Gronwall's lemma, using (2.5a), (2.5b), (2.5c), and choosing α small, we arrive at the desired result. \square

Theorem 3.6. *The fully-discrete problem (3.1) satisfies the energy estimate*

$$\|\mathbf{u}_h\|_{l^\infty(H^1)}^2 + \|p_h\|_{l^\infty(J)}^2 + \|\mathbf{z}_h\|_{l^2(L_2)}^2 + \|p_h\|_{l^2(L_2)}^2 + \|\nabla \cdot \mathbf{z}_h\|_{l^2(L_2)}^2 \leq C.$$

Proof. The proof follows from combining lemma 3.3 and lemma 3.5, and noting that these lemmas hold for all time steps $n = 0, 1, \dots, N$. This then gives the desired l^∞ bounds. \square

Remark 1. *Having proven Theorem 3.6, it is now a standard calculation to show that the discrete Galerkin approximation converges weakly to the continuous problem with respect to the norms of the energy estimate in Theorem 3.6. This in turn shows that the continuous variational problem is well-posed. Due to the linearity of the variational form and noting that $\|\mathbf{v}\|_{J,\Omega} \rightarrow 0$ as $h \rightarrow 0$, these calculations are straight forward and closely follow the existence and uniqueness proofs presented in [43] and [5] for the linear two-field Biot problem and a nonlinear Biot problem, respectively.*

4 A-priori error analysis

We now derive an a-priori error estimate for the fully-discrete model. We start by introducing some notation, and then give a Galerkin orthogonality result which will form the corner stone of the error analysis. We then present some useful approximation results, and prove some lemmas for the finite element error, before closing the section with the final error estimate, Theorem 4.5. To ease the notation we introduce the following interpolation errors:

$$\boldsymbol{\eta}_{\mathbf{u}}^n := \mathbf{u}(t_n) - \pi_h \mathbf{u}(t_n), \boldsymbol{\eta}_{\mathbf{u}_t}^n := \mathbf{u}_t(t_n) - \pi_h \mathbf{u}_t(t_n), \boldsymbol{\eta}_{\mathbf{z}}^n := \mathbf{z}(t_n) - \pi_h \mathbf{z}(t_n), \eta_p^n := p(t_n) - \pi_h p(t_n), \quad (4.1)$$

auxiliary errors:

$$\boldsymbol{\theta}_{\mathbf{u}}^n := \pi_h \mathbf{u}(t_n) - \mathbf{u}_h^n, \boldsymbol{\theta}_{\mathbf{z}}^n := \pi_h \mathbf{z}(t_n) - \mathbf{z}_h^n, \theta_p^n := \pi_h p(t_n) - p_h^n, \quad (4.2)$$

and time-discretization errors:

$$\boldsymbol{\rho}_{\mathbf{u}}^n := \frac{\mathbf{u}(t_n) - \mathbf{u}(t_{n-1})}{\Delta t} - \frac{\partial \mathbf{u}(t_n)}{\partial t}, \rho_p^n := \frac{p(t_n) - p(t_{n-1})}{\Delta t} - \frac{\partial p(t_n)}{\partial t}. \quad (4.3)$$

4.1 Galerkin orthogonality

We now give a Galerkin orthogonality type argument for analysing the difference between the approximated fully-discrete solution and the true continuous solution. For this we introduce the continuous counterpart of the fully-discrete combined weak form (3.18) given by

$$B^n[(\mathbf{u}, \mathbf{z}, p), (\mathbf{v}, \mathbf{w}, q)] = (\mathbf{f}(t_n), \mathbf{v}) + (\mathbf{t}_N(t_n), \mathbf{v})_{\Gamma_t} + (\mathbf{b}(t_n), \mathbf{w}) - (p_D, \mathbf{w} \cdot \mathbf{n})_{\Gamma_p} + (g(t_n), q) \quad \forall (\mathbf{v}, \mathbf{w}, q) \in \mathcal{V}_h^X,$$

where

$$B^n[(\mathbf{u}, \mathbf{z}, p), (\mathbf{v}, \mathbf{w}, q)] = a(\mathbf{u}(t_n), \mathbf{v}) + \boldsymbol{\kappa}^{-1}(\mathbf{z}(t_n), \mathbf{w}) - (p(t_n), \nabla \cdot \mathbf{v}) - (p(t_n), \nabla \cdot \mathbf{w}) + (\nabla \cdot \mathbf{u}_t(t_n), q) + (\nabla \cdot \mathbf{z}(t_n), q).$$

Lemma 4.1. *If $(\mathbf{u}(t_n), \mathbf{z}(t_n), p(t_n))$ is a solution to (4.4) with $(\mathbf{u}(t_n), \mathbf{z}(t_n), p(t_n)) \in \mathbf{W}^E \times \mathbf{W}^D \times H^1(\Omega) \cap L^2$ then*

$$B_h^n[(\mathbf{u} - \mathbf{u}_h, \mathbf{z} - \mathbf{z}_h, p - p_h), (\mathbf{v}_h, \mathbf{w}_h, q_h)] = (\nabla \cdot \boldsymbol{\rho}_{\mathbf{u}}^n, q_h) + J(\rho_p^n, q_h) \quad \forall (\mathbf{v}_h, \mathbf{w}_h, q_h) \in \mathcal{V}_h^X.$$

Proof. Subtracting the discrete weak form (3.5) from the continuous weak form (4.4) we have

$$B^n[(\mathbf{u}, \mathbf{z}, p), (\mathbf{v}_h, \mathbf{w}_h, q_h)] - B_h^n[(\mathbf{u}_h, \mathbf{z}_h, p_h), (\mathbf{v}_h, \mathbf{w}_h, q_h)] = 0,$$

which gives us

$$a(\mathbf{u}(t_n) - \mathbf{u}_h^n, \mathbf{v}_h) + (\boldsymbol{\kappa}^{-1}(\mathbf{z}(t_n) - \mathbf{z}_h^n), \mathbf{w}_h) - (p(t_n) - p_h^n, \nabla \cdot \mathbf{v}_h) - (p(t_n) - p_h^n, \nabla \cdot \mathbf{w}_h) + (\nabla \cdot (\mathbf{z}(t_n) - \mathbf{z}_h^n), q_h^n) + (\nabla \cdot (\mathbf{u}_t(t_n) - \mathbf{u}_{\delta t_h}^n), q_h) - J(p_{\delta t_h}^n, q_h) = 0.$$

Now add $J(p_t(t_n), q) = 0$ to the left hand side. Here we have made the additional assumption that $p(t_n) \in H^1(\Omega)$, so that $[p_t(t_n)] = 0$. Also add $(\nabla \cdot (\mathbf{u}_{\delta t}(t_n) - \mathbf{u}_t(t_n)), q) + J(p_{\delta t}(t_n) - p_t(t_n), q)$ to the left and the right hand side to yield

$$\begin{aligned} a(\mathbf{u}(t_n) - \mathbf{u}_h^n, \mathbf{v}) + (\boldsymbol{\kappa}^{-1}(\mathbf{z}(t_n) - \mathbf{z}_h^n), \mathbf{w}_h) - (p(t_n) - p_h^n, \nabla \cdot \mathbf{v}_h) - (p(t_n) - p_h^n, \nabla \cdot \mathbf{w}_h) + (\nabla \cdot (\mathbf{z}(t_n) - \mathbf{z}_h^n), q) \\ + (\nabla \cdot (\mathbf{u}_{\delta t}(t_n) - \mathbf{u}_{\delta t_h}^n), q) + J(p_{\delta t}(t_n) - p_{\delta t_h}^n, q_h) = (\nabla \cdot (\mathbf{u}_{\delta t}(t_n) - \mathbf{u}_t(t_n)), q_h) \\ + J(p_{\delta t}(t_n) - p_t(t_n), q_h). \end{aligned} \quad (4.4)$$

The result now follows. \square

4.2 Approximation results

We now give some approximation results that will be useful later.

Lemma 4.2. *The projection operator π_h has the following approximation property for functions $(\mathbf{u}(t_n), \mathbf{z}(t_n), p(t_n)) \in [H^2(\Omega)]^d \times [H^1(\Omega)]^d \times H^1(\Omega)$:*

$$\|\boldsymbol{\eta}_{\mathbf{u}}^n\|_{1,\Omega} \leq Ch\|\mathbf{u}^n\|_{2,\Omega}, \quad \|\boldsymbol{\eta}_{\mathbf{z}}^n\|_{0,\Omega} \leq Ch\|\mathbf{z}^n\|_{1,\Omega}, \quad \|\eta_p^n\|_{0,\Omega} \leq Ch\|p^n\|_{1,\Omega}. \quad (4.5)$$

We also have the following approximation for the time-discretization error:

$$\sum_{n=1}^N \Delta t \|\boldsymbol{\rho}_{\mathbf{u}}^n\|_{0,\Omega}^2 \leq \Delta t^2 \int_0^{t_N} \|\mathbf{u}_{tt}\|_{0,\Omega}^2 ds. \quad (4.6)$$

Proof. Straight from standard approximation theory in [8] and [36]. \square

Lemma 4.3. *Assume that the true solution $(\mathbf{u}, \mathbf{z}, p)$ is in $H^2([H^2(\Omega)]^d) \times l^2([H^1(\Omega)]^d) \times H^2(H^1(\Omega) \cap L^2)$, then the finite element solution (3.1) satisfies the error estimate*

$$\begin{aligned} \|\boldsymbol{\theta}_{\mathbf{u}}\|_{l^\infty(H^1)} + \|\boldsymbol{\theta}_{\mathbf{z}}\|_{l^2(L^2)} + \|\theta_p\|_{l^\infty(L^2)} + \|\theta_p\|_{l^\infty(J)} \\ \leq Ch \left(\|p_t\|_{l^2(H^1)} + \|\mathbf{u}\|_{l^\infty(H^2)}^2 + \|\mathbf{u}_t\|_{l^2(H^2)} + \|\mathbf{z}\|_{l^2(H^1)} \right) + Ch\Delta t \left(\|\mathbf{u}_{tt}\|_{L^2(H^2)} + \|p_{tt}\|_{L^2(H^1)} \right) \\ + C\Delta t \left(\|p_{tt}\|_{L^2(L^2)}^2 + \|\nabla \cdot \mathbf{u}_{tt}\|_{L^2(L^2)}^2 \right). \end{aligned}$$

Proof. From the Galerkin orthogonality result, lemma 4.1, we have

$$\begin{aligned} a(\mathbf{u}^n - \mathbf{u}_h^n, \mathbf{v}_h) + (\boldsymbol{\kappa}^{-1}(\mathbf{z}^n - \mathbf{z}_h^n), \mathbf{w}_h) - (p^n - p_h^n, \nabla \cdot \mathbf{v}_h) - (p^n - p_h^n, \nabla \cdot \mathbf{w}_h) \\ + (q_h, \nabla \cdot (\mathbf{z}^n - \mathbf{z}_h^n)) + (q_h, \nabla \cdot (\mathbf{u}_{\delta t}^n - \mathbf{u}_{\delta t_h}^n)) + J(p_{\delta t}^n - p_{\delta t_h}^n, q_h) \\ = (\nabla \cdot \boldsymbol{\rho}_{\mathbf{u}}^n, q_h) + J(\rho_p^n, q_h). \end{aligned}$$

Using the definitions of the interpolation error (4.1) and the auxiliary error (4.2), and choosing $\mathbf{v}_h = \boldsymbol{\theta}_{\delta t \mathbf{u}}^n + \pi_h \mathbf{v}_p$, $\mathbf{w}_h = \boldsymbol{\theta}_{\mathbf{z}}^n$, $q_h = \theta_p^n$, with $-\nabla \cdot \mathbf{v}_p = \theta_p^n$, we get

$$\begin{aligned} a(\boldsymbol{\theta}_{\mathbf{u}}^n + \boldsymbol{\eta}_{\mathbf{u}}^n, \boldsymbol{\theta}_{\delta t \mathbf{u}}^n + \pi_h \mathbf{v}_p) + (\boldsymbol{\kappa}^{-1}(\boldsymbol{\theta}_{\mathbf{z}}^n + \boldsymbol{\eta}_{\mathbf{z}}^n), \boldsymbol{\theta}_{\mathbf{z}}^n) - (\theta_p^n + \eta_p^n, \nabla \cdot \boldsymbol{\theta}_{\delta t \mathbf{u}}^n) - (\theta_p^n + \eta_p^n, \nabla \cdot \boldsymbol{\theta}_{\mathbf{z}}^n + \pi_h \mathbf{v}_p) \\ + (\theta_p^n, \nabla \cdot (\boldsymbol{\theta}_{\mathbf{z}}^n + \boldsymbol{\eta}_{\mathbf{z}}^n)) + (\theta_p^n, \nabla \cdot (\boldsymbol{\theta}_{\delta t \mathbf{u}}^n + \boldsymbol{\eta}_{\delta t \mathbf{u}}^n)) + J(\theta_{\delta t p}^n + \eta_{\delta t p}^n, \theta_p^n) \\ = (\nabla \cdot \boldsymbol{\rho}_{\mathbf{u}}^n, \theta_p^n) + J(\rho_p^n, \theta_p^n). \end{aligned}$$

Rearranging, noting that $(\eta_p^n, \nabla \cdot \boldsymbol{\theta}_{\delta tu}^n + \pi_h \mathbf{v}_p) = (\eta_p^n, \nabla \cdot \boldsymbol{\theta}_z^n) = 0$, multiplying both sides by Δt and summing we have

$$\begin{aligned} \sum_{n=1}^N \Delta t a(\boldsymbol{\theta}_u^n, \boldsymbol{\theta}_{\delta tu}^n) + \sum_{n=1}^N \Delta t (\boldsymbol{\kappa}^{-1}(\boldsymbol{\theta}_z^n, \boldsymbol{\theta}_z^n)) + \sum_{n=1}^N \Delta t a(\boldsymbol{\theta}_u^n, \pi_h \mathbf{v}_p) - \sum_{n=1}^N \Delta t (\theta_p^n, \nabla \cdot \pi_h \mathbf{v}_p) \\ + \sum_{n=1}^N \Delta t J(\theta_{\delta tp}^n, \theta_p^n) = \Phi_1 + \Phi_2 + \Phi_3 + \Phi_4 + \Phi_5 + \Phi_6. \end{aligned} \quad (4.7)$$

where

$$\begin{aligned} \Phi_1 &= - \sum_{n=1}^N \Delta t a(\boldsymbol{\eta}_u^n, \boldsymbol{\theta}_{\delta tu}^n), & \Phi_2 &= - \sum_{n=1}^N \Delta t (\boldsymbol{\kappa}^{-1}(\boldsymbol{\eta}_z^n, \boldsymbol{\theta}_z^n)), & \Phi_3 &= - \sum_{n=1}^N \Delta t a(\boldsymbol{\eta}_u^n, \pi_h \mathbf{v}_p), \\ \Phi_4 &= - \sum_{n=1}^N \Delta t J(\eta_{\delta tp}^n, \theta_p^n), & \Phi_5 &= \sum_{n=1}^N \Delta t (\nabla \cdot \boldsymbol{\rho}_u^n, \theta_p^n), & \Phi_6 &= \sum_{n=1}^N \Delta t J(\rho_p^n, \theta_p^n). \end{aligned}$$

Using (3.25) we can immediately bound the left hand side terms of (4.7) such that

$$\begin{aligned} \frac{C_k}{2} \|\boldsymbol{\theta}_u^N\|_{1,\Omega}^2 + \frac{1}{2} \|\theta_p^N\|_{J,\Omega}^2 + \lambda_{max}^{-1} \|\boldsymbol{\theta}_z\|_{l^2(L_2)}^2 + (1 - C\alpha) \|\theta_p\|_{l^2(L_2)}^2 - \frac{C_c}{2\alpha} \|\boldsymbol{\theta}_u\|_{l^2(H^1)}^2 - \frac{1}{4\alpha} \|\theta_p\|_{l^2(J)}^2 \\ \leq \sum_{n=1}^N \Delta t a(\boldsymbol{\theta}_u^n, \boldsymbol{\theta}_{\delta tu}^n) + \sum_{n=1}^N \Delta t (\boldsymbol{\kappa}^{-1}(\boldsymbol{\theta}_z^n, \boldsymbol{\theta}_z^n)) + \sum_{n=1}^N \Delta t a(\boldsymbol{\theta}_u^n, \pi_h \mathbf{v}_p) \\ - \sum_{n=1}^N \Delta t (\theta_p^n, \nabla \cdot \pi_h \mathbf{v}_p) + \sum_{n=1}^N \Delta t J(\theta_{\delta tp}^n, \theta_p^n). \end{aligned} \quad (4.8)$$

Here we have also used that $\boldsymbol{\theta}_u^0 = 0$ due to (3.2a). We now move to the terms on the right hand side of (4.7). We will bound these primarily using the Cauchy-Schwarz and Young's inequalities. To bound the first quantity, we use (3.26), lemma 4.2, the Cauchy-Schwarz and Young's inequalities, and (2.2),

$$\begin{aligned} \Phi_1 &= - \sum_{n=1}^N a(\boldsymbol{\eta}_u^n, \boldsymbol{\theta}_u^n - \boldsymbol{\theta}_u^{n-1}) \\ &= a(\boldsymbol{\eta}_u^N, \boldsymbol{\theta}_u^N) - \sum_{n=1}^N a(\boldsymbol{\eta}_u^n - \boldsymbol{\eta}_u^{n-1}, \boldsymbol{\theta}_u^n) \\ &= a(\boldsymbol{\eta}_u^N, \boldsymbol{\theta}_u^N) - \Delta t \sum_{n=1}^N a(\boldsymbol{\eta}_{u_t}^n, \boldsymbol{\theta}_u^n) - \sum_{n=1}^N a\left(\int_{t_{n-1}}^{t_n} (s - t_{n-1}) \boldsymbol{\eta}_{u_{tt}} ds, \boldsymbol{\theta}_u^n\right) \\ &\leq \frac{\alpha C_c}{2} \|\boldsymbol{\theta}_u^N\|_{1,\Omega}^2 + \frac{C_c}{2\alpha} \|\boldsymbol{\eta}_u^N\|_{1,\Omega}^2 + \alpha C_c \|\boldsymbol{\theta}_u\|_{l^2(H^1)}^2 + \frac{C_c}{2\alpha} \|\boldsymbol{\eta}_{u_t}\|_{l^2(H^1)}^2 + \frac{C_c}{2\alpha} \Delta t^2 \int_0^{t_N} \|\boldsymbol{\eta}_{u_{tt}}\|_{1,\Omega}^2 ds. \end{aligned} \quad (4.9)$$

Next, using (2.3), and Young's inequality,

$$\Phi_2 \leq \frac{\alpha}{2} \|\boldsymbol{\theta}_z\|_{l^2(L_2)}^2 + \frac{\lambda_{min}^{-2}}{2\alpha} \|\boldsymbol{\eta}_z^n\|_{l^2(L_2)}^2. \quad (4.10)$$

Again using (2.2), Young's inequality, and (3.12),

$$\Phi_3 \leq \frac{\alpha}{2} \|\pi_h \mathbf{v}_p\|_{l^2(H^1)}^2 + \frac{C_c^2}{2\alpha} \|\boldsymbol{\eta}_{\mathbf{u}}\|_{l^2(H^1)}^2 \leq \frac{\alpha \hat{c}^2}{2} \|\theta_p\|_{l^2(L_2)}^2 + \frac{C_c^2}{2\alpha} \|\boldsymbol{\eta}_{\mathbf{u}}^n\|_{l^2(H^1)}^2. \quad (4.11)$$

The next bound is obtained using workings similar to (4.9),

$$\Phi_4 \leq \alpha \|\theta_p\|_{l^2(J)}^2 + \frac{1}{2\alpha} \|\eta_{pt}\|_{l^2(J)}^2 + \frac{\Delta t^2}{2\alpha} \int_0^{t_N} \|\eta_{ptt}\|_{J,\Omega}^2 ds. \quad (4.12)$$

Using the Cauchy-Schwarz and Young's inequalities and lemma 4.2,

$$\Phi_5 \leq \frac{\alpha}{2} \|\theta_p\|_{l^2(L_2)}^2 + \frac{1}{2\alpha} \sum_{n=1}^N \Delta t \|\nabla \cdot \boldsymbol{\rho}_{\mathbf{u}}^n\|_{0,\Omega}^2 \leq \frac{\alpha}{2} \|\theta_p\|_{l^2(L_2)}^2 + \frac{\Delta t^2}{2\alpha} \int_0^{t_N} \|\nabla \cdot \mathbf{u}_{tt}\|_{0,\Omega}^2 ds. \quad (4.13)$$

Similarly we have

$$\Phi_6 \leq \frac{\alpha}{2} \|\theta_p\|_{l^2(J)}^2 + \frac{\Delta t^2}{2\alpha} \int_0^{t_N} \|p_{tt}\|_{J,\Omega}^2 ds. \quad (4.14)$$

We can now combine the individual bounds (4.9), (4.10), (4.11), (4.12), (4.13), (4.14), with (4.8) to obtain from (4.7),

$$\begin{aligned} & \left(\frac{C_k}{2} - \frac{C_c \alpha}{2} \right) \|\boldsymbol{\theta}_{\mathbf{u}}^N\|_{1,\Omega}^2 + \frac{1}{2} \|\theta_p^N\|_{J,\Omega}^2 + \lambda_{max}^{-1} \|\boldsymbol{\theta}_{\mathbf{z}}\|_{l^2(L_2)}^2 + (1 - C\alpha) \|\theta_p\|_{l^2(L_2)}^2 \\ & \leq C_c \left(\frac{1}{2\alpha} + \alpha \right) \|\boldsymbol{\theta}_{\mathbf{u}}\|_{l^2(H^1)}^2 + \left(\alpha + \frac{\alpha}{2} + \frac{1}{4\alpha} \right) \|\theta_p\|_{l^2(J)}^2 + \frac{1}{2\alpha} \|\eta_{pt}\|_{l^2(J)}^2 \\ & \quad + \frac{1}{2\alpha} \left(C_c \|\boldsymbol{\eta}_{\mathbf{u}_t}\|_{l^2(H^1)}^2 + C_c \|\boldsymbol{\eta}_{\mathbf{u}}^N\|_{1,\Omega}^2 + \lambda_{min}^{-2} \|\boldsymbol{\eta}_{\mathbf{z}}\|_{l^2(L_2)}^2 + C_c^2 \|\boldsymbol{\eta}_{\mathbf{u}}\|_{l^2(H^1)}^2 \right) \\ & \quad + \frac{\Delta t^2}{2\alpha} \left(\int_0^{t_N} C_c \|\boldsymbol{\eta}_{\mathbf{u}_{tt}}\|_{1,\Omega}^2 ds + \int_0^{t_N} \|\eta_{ptt}\|_{J,\Omega}^2 ds + \int_0^{t_N} \|\nabla \cdot \mathbf{u}_{tt}\|_{0,\Omega}^2 ds + \int_0^{t_N} \|p_{tt}\|_{J,\Omega}^2 ds \right). \end{aligned} \quad (4.15)$$

Now choosing α sufficiently small, and applying a discrete version of Gronwall's lemma, we get

$$\begin{aligned} \|\boldsymbol{\theta}_{\mathbf{u}}^N\|_{1,\Omega}^2 + \|\theta_p^N\|_{J,\Omega}^2 + \|\boldsymbol{\theta}_{\mathbf{z}}\|_{l^2(L_2)}^2 + \|\theta_p\|_{l^2(L_2)}^2 & \leq C \left(\|\eta_{pt}\|_{l^2(J)}^2 + \|\boldsymbol{\eta}_{\mathbf{u}}^N\|_{1,\Omega}^2 + \|\boldsymbol{\eta}_{\mathbf{u}_t}\|_{l^2(H^1)}^2 + \|\boldsymbol{\eta}_{\mathbf{z}}\|_{l^2(L_2)}^2 \right) \\ & \quad + C \Delta t^2 \left(\|\boldsymbol{\eta}_{\mathbf{u}_{tt}}\|_{L^2(H^1)}^2 + \|\eta_{ptt}\|_{L^2(J)}^2 \right) \\ & \quad + C \Delta t^2 \left(\|\nabla \cdot \mathbf{u}_{tt}\|_{L^2(L_2)}^2 + \|p_{tt}\|_{L^2(J)}^2 \right). \end{aligned}$$

Now applying approximation results for the projection (4.2), the bound (3.3), and taking the square rooting on both sides, we have

$$\begin{aligned} \|\boldsymbol{\theta}_{\mathbf{u}}^N\|_{1,\Omega} + \|\theta_p^N\|_{J,\Omega} + \|\boldsymbol{\theta}_{\mathbf{z}}\|_{l^2(L_2)} + \|\theta_p\|_{l^2(L_2)} & \leq Ch \left(\|p_{tt}\|_{l^2(H^1)} + \|\mathbf{u}^N\|_{2,\Omega} + \|\mathbf{u}_t\|_{l^2(H^2)} + \|\mathbf{z}\|_{l^2(H^1)} \right) \\ & \quad + Ch \Delta t \left(\|\mathbf{u}_{tt}\|_{L^2(H^2)} + \|p_{tt}\|_{L^2(H^1)} \right) \\ & \quad + C \Delta t \left(\|\nabla \cdot \mathbf{u}_{tt}\|_{L^2(L_2)} + \|p_{tt}\|_{L^2(L_2)} \right). \end{aligned}$$

Because the above holds for all time steps $n = 0, 1, \dots, N$, we can get the desired l^∞ bounds to complete the proof of the theorem. \square

We now present an a-priori auxillary error estimate of the fluid flux, in its natural $Hdiv$ norm. To our knowledge no previous papers have been able to show convergence of a finite element method solving the three-field poroelastic equations in this norm. This result is due to the coercivity given in Theorem 3.1.

Lemma 4.4. *Assume that the true solution $(\mathbf{u}, \mathbf{z}, p)$ is in $H^2\left([H^2(\Omega)]^d\right) \times H^1\left([H^2(\Omega)]^d\right) \cap H^2\left([H^1(\Omega)]^d\right) \times H^2\left(H^1(\Omega) \cap L^2\right)$, then the finite element solution (3.1) satisfies the auxillary error estimate*

$$\begin{aligned} \|\nabla \cdot \boldsymbol{\theta}_z\|_{L^2(L_2)} &\leq Ch \left(\|\mathbf{u}_t\|_{L^2(H^2)} + \|\nabla \cdot \mathbf{z}\|_{L^2(H^1)} + \|\nabla \cdot \mathbf{z}_t\|_{L^2(H^1)} + \|p_t\|_{L^2(H^1)} + \|\mathbf{z}\|_{L^2(H^1)} \right) \\ &\quad + Ch\Delta t \left(\|\nabla \cdot \mathbf{u}_{tt}\|_{L^2(H^1)} + \|\mathbf{z}_{tt}\|_{L^2(H^1)} + \|p_{tt}\|_{L^2(H^1)} \right) \\ &\quad + C\Delta t \left(\|p_{tt}\|_{L^2(L_2)} + \|\nabla \cdot \mathbf{u}_{tt}\|_{L^2(L_2)} \right). \end{aligned}$$

Proof. This proof is very similar to the previous proof. We will therefore only show the main intermediate results. We can get the following Galerkin orthogonality by subtracting the fully-discrete weak formulation (3.1) from the continuous formulation (2.4),

$$a(\mathbf{u}(t_n) - \mathbf{u}_h^n, \mathbf{v}_h) - (p(t_n) - p_h^n, \nabla \cdot \mathbf{v}_h) = 0 \quad \forall \mathbf{v}_h \in \mathbf{W}_{h0}^E, \quad (4.16a)$$

$$(\boldsymbol{\kappa}^{-1}(\mathbf{z}(t_n) - \mathbf{z}_h^n), \mathbf{w}_h) - (p(t_n) - p_h^n, \nabla \cdot \mathbf{w}_h) = 0 \quad \forall \mathbf{w}_h \in \mathbf{W}_{h0}^D, \quad (4.16b)$$

$$(\nabla \cdot (\mathbf{u}_{\delta t}(t_n) - \mathbf{u}_{\delta t_h}^n) + \nabla \cdot (\mathbf{z}(t_n) - \mathbf{z}_h^n), q_h) + J(p_t(t_n) - p_{\delta t_h}^n, q_h) = (\nabla \cdot \boldsymbol{\rho}_u^n, q_h) + J(\rho_p^n, q_h) \quad \forall q_h \in Q_h. \quad (4.16c)$$

Note that this also holds at the previous time step such that

$$a(\mathbf{u}(t_{n-1}) - \mathbf{u}_h^{n-1}, \mathbf{v}_h) - (p(t_{n-1}) - p_h^{n-1}, \nabla \cdot \mathbf{v}_h) = 0 \quad \forall \mathbf{v}_h \in \mathbf{W}_{h0}^E, \quad (4.17a)$$

$$(\boldsymbol{\kappa}^{-1}(\mathbf{z}(t_{n-1}) - \mathbf{z}_h^{n-1}), \mathbf{w}_h) - (p(t_{n-1}) - p_h^{n-1}, \nabla \cdot \mathbf{w}_h) = 0 \quad \forall \mathbf{w}_h \in \mathbf{W}_{h0}^D. \quad (4.17b)$$

Subtracting (4.17a) from (4.16a) and dividing by Δt , and performing a similar operation for (4.17b) and (4.16b), we obtain

$$a(\mathbf{u}_{\delta t}(t_n) - \mathbf{u}_{\delta t_h}^n, \mathbf{v}_h) - (p_{\delta t}(t_n) - p_{\delta t_h}^n, \nabla \cdot \mathbf{v}_h) = 0 \quad \forall \mathbf{v}_h \in \mathbf{W}_{h0}^E, \quad (4.18a)$$

$$(\boldsymbol{\kappa}^{-1}(\mathbf{z}_{\delta t}(t_n) - \mathbf{z}_{\delta t_h}^n), \mathbf{w}_h) - (p_{\delta t}(t_n) - p_{\delta t_h}^n, \nabla \cdot \mathbf{w}_h) = 0 \quad \forall \mathbf{w}_h \in \mathbf{W}_{h0}^D, \quad (4.18b)$$

$$(\nabla \cdot (\mathbf{u}_{\delta t}(t_n) - \mathbf{u}_{\delta t_h}^n), q_h) + (\nabla \cdot (\mathbf{z}(t_n) - \mathbf{z}_h^n), q_h) + J(p_t(t_n) - p_{\delta t_h}^n, q_h) = (\nabla \cdot \boldsymbol{\rho}_u^n, q_h) + J(\rho_p^n, q_h) \quad \forall q_h \in Q_h. \quad (4.18c)$$

Now noting that we can write the error as $\mathbf{u}_{\delta t}^n - \mathbf{u}_{\delta t_h}^n = (\mathbf{u}_{\delta t}^n - \pi_h \mathbf{u}_{\delta t}^n) + (\pi_h \mathbf{u}_{\delta t}^n - \mathbf{u}_{\delta t_h}^n) = \boldsymbol{\eta}_{\delta t \mathbf{u}}^n + \boldsymbol{\theta}_{\delta t \mathbf{u}}^n$ and similarly for the other variables. Choosing $\mathbf{v}_h = \beta \boldsymbol{\theta}_{\delta t \mathbf{u}}^n$, $\mathbf{w}_h = \beta \boldsymbol{\theta}_{\delta t \mathbf{z}}^n$, $q_h = \beta \theta_{\delta t p}^n + \nabla \cdot \boldsymbol{\theta}_{\delta t \mathbf{z}}^n$, adding (4.18a), (4.18b) and (4.18c), rearranging, multiplying by Δt , and summing we have,

$$\sum_{n=1}^N \Delta t B_h^*[(\boldsymbol{\theta}_{\mathbf{u}}^n, \boldsymbol{\theta}_{\mathbf{z}}^n, \theta_p^n), (\beta \boldsymbol{\theta}_{\delta t \mathbf{u}}^n, \beta \boldsymbol{\theta}_{\delta t \mathbf{z}}^n, \beta \theta_{\delta t p}^n)] = \Psi_1 + \Psi_2 + \Psi_3 + \Psi_4 + \Psi_5 + \Psi_6, \quad (4.19)$$

where

$$\begin{aligned}
\Psi_1 &= - \sum_{n=1}^N \Delta t a(\boldsymbol{\eta}_{\delta t \mathbf{u}}^n, \beta \boldsymbol{\theta}_{\delta t \mathbf{u}}^n), & \Psi_2 &= - \sum_{n=1}^N \Delta t (\nabla \cdot (\boldsymbol{\eta}_{\delta t \mathbf{u}}^n + \boldsymbol{\eta}_{\mathbf{z}}^n), \nabla \cdot \boldsymbol{\theta}_{\mathbf{z}}^n), \\
\Psi_3 &= \sum_{n=1}^N \Delta t J(\boldsymbol{\eta}_{\delta t \mathbf{p}}^n, \nabla \cdot \boldsymbol{\theta}_{\mathbf{z}}^n - \beta \boldsymbol{\theta}_{\delta t \mathbf{p}}^n), & \Psi_4 &= - \sum_{n=1}^N \Delta t (\boldsymbol{\kappa}^{-1}(\boldsymbol{\eta}_{\delta t \mathbf{z}}^n, \beta \boldsymbol{\theta}_{\mathbf{z}}^n)), \\
\Psi_5 &= \sum_{n=1}^N \Delta t J(\rho_{\mathbf{p}}^n, \beta \boldsymbol{\theta}_{\delta t \mathbf{p}}^n + \nabla \cdot \boldsymbol{\theta}_{\mathbf{z}}^n), & \Psi_6 &= \sum_{n=1}^N \Delta t (\nabla \cdot \boldsymbol{\rho}_{\mathbf{u}}^n, \beta \boldsymbol{\theta}_{\delta t \mathbf{p}}^n + \nabla \cdot \boldsymbol{\theta}_{\mathbf{z}}^n).
\end{aligned}$$

Using (3.39) we can immediately bound the left hand side of (4.19), such that

$$\begin{aligned}
& \left(\beta C_k - \frac{C_p}{2\alpha} \right) \|\boldsymbol{\theta}_{\delta t \mathbf{u}}\|_{l^2(H^1)}^2 + \frac{\beta \lambda_{\max}^{-1}}{2} \|\boldsymbol{\theta}_{\mathbf{z}}^N\|_{0,\Omega}^2 + \left(\beta - \frac{1}{2\alpha} \right) \|\boldsymbol{\theta}_{\delta t \mathbf{p}}\|_{l^2(J)}^2 + (1 - \alpha(1 + c_z)) \|\nabla \cdot \boldsymbol{\theta}_{\mathbf{z}}\|_{l^2(L_2)}^2 \\
& \leq \sum_{n=1}^N \Delta t B_h^*[(\boldsymbol{\theta}_{\mathbf{u}}^n, \boldsymbol{\theta}_{\mathbf{z}}^n, \theta_p^n), (\beta \boldsymbol{\theta}_{\delta t \mathbf{u}}^n, \beta \boldsymbol{\theta}_{\mathbf{z}}^n, \beta \boldsymbol{\theta}_{\delta t \mathbf{u}}^n)]. \quad (4.20)
\end{aligned}$$

Here we have also assumed that $\boldsymbol{\theta}_{\mathbf{z}}^0 = 0$. We now bound the terms on the right hand side of (4.19) using machinery developed during previous proofs.

$$\Psi_1 \leq \frac{C_c \alpha}{2} \|\boldsymbol{\theta}_{\delta t \mathbf{u}}\|_{l^2(H^1)}^2 + \frac{\beta^2 C_c}{2\alpha} \|\boldsymbol{\eta}_{\mathbf{u}t}\|_{l^2(H^1)}^2 + \frac{\beta^2 C_c \Delta t^2}{2\alpha} \int_0^{t_N} \|\boldsymbol{\eta}_{\mathbf{u}tt}\|_{1,\Omega}^2 ds, \quad (4.21)$$

$$\Psi_2 \leq \frac{1}{2\alpha} \|\nabla \cdot \boldsymbol{\eta}_{\mathbf{z}}\|_{l^2(L_2)}^2 + \alpha \|\nabla \cdot \boldsymbol{\theta}_{\mathbf{z}}\|_{l^2(L_2)}^2 + \frac{1}{2\alpha} \|\nabla \cdot \boldsymbol{\eta}_{\mathbf{u}t}\|_{l^2(L_2)}^2 + \frac{\Delta t^2}{2\alpha} \int_0^{t_N} \|\nabla \cdot \boldsymbol{\eta}_{\mathbf{u}tt}\|_{0,\Omega}^2 ds, \quad (4.22)$$

$$\begin{aligned}
\Psi_3 &\leq \alpha c_z \|\nabla \cdot \boldsymbol{\theta}_{\mathbf{z}}\|_{l^2(L_2)}^2 + \frac{\alpha}{2} \|\boldsymbol{\theta}_{\delta t \mathbf{p}}^n\|_{l^2(J)}^2 \\
&\quad + \frac{1 + \beta^2}{2\alpha} \|\boldsymbol{\eta}_{\mathbf{p}t}\|_{l^2(J)}^2 + \frac{(1 + \beta^2) \Delta t^2}{2\alpha} \int_0^{t_N} \|\boldsymbol{\eta}_{\mathbf{p}tt}\|_{J,\Omega}^2 ds, \quad (4.23)
\end{aligned}$$

$$\Psi_4 \leq \frac{\alpha}{2} \|\boldsymbol{\theta}_{\mathbf{z}}\|_{l^2(L_2)}^2 + \frac{\lambda_{\min}^{-2} \beta^2}{2\alpha} \left(\|\boldsymbol{\eta}_{\mathbf{z}t}\|_{l^2(L_2)}^2 + \Delta t^2 \int_0^{t_N} \|\boldsymbol{\eta}_{\mathbf{z}tt}\|_{0,\Omega}^2 ds \right), \quad (4.24)$$

$$\Psi_5 \leq \frac{\alpha}{2} \|\boldsymbol{\theta}_{\delta t \mathbf{p}}\|_{l^2(J)}^2 + \alpha c_z \|\nabla \cdot \boldsymbol{\theta}_{\mathbf{z}}\|_{l^2(L_2)}^2 + \frac{(1 + \beta^2) \Delta t^2}{2\alpha} \int_0^{t_N} \|\boldsymbol{p}_{tt}\|_{J,\Omega}^2 ds, \quad (4.25)$$

$$\Psi_6 \leq \frac{\alpha}{2} \|\boldsymbol{\theta}_{\delta t \mathbf{p}}\|_{l^2(L_2)}^2 + \frac{\alpha}{2} \|\nabla \cdot \boldsymbol{\theta}_{\mathbf{z}}\|_{l^2(L_2)}^2 + \frac{(1 + \beta^2) \Delta t^2}{2\alpha} \int_0^{t_N} \|\nabla \cdot \boldsymbol{u}_{tt}\|_{0,\Omega}^2 ds. \quad (4.26)$$

We can now combine the individual bounds (4.21), (4.22), (4.23), (4.24), (4.25), with (4.20) to obtain from (4.19),

$$\begin{aligned}
& \left(\beta C_k - \frac{C_p}{2\alpha} - \frac{C_c \alpha}{2} \right) \|\boldsymbol{\theta}_{\delta t \mathbf{u}}\|_{l^2(H^1)}^2 + \frac{\lambda_{max}^{-1} \beta}{2} \|\boldsymbol{\theta}_{\mathbf{z}}^N\|_{0,\Omega}^2 + \left(1 - \frac{5\alpha}{2} - 2\alpha c_z \right) \|\nabla \cdot \boldsymbol{\theta}_{\mathbf{z}}\|_{l^2(L_2)}^2 \\
& + \left(\beta - \frac{1}{2\alpha} - \frac{3\alpha}{2} \right) \|\boldsymbol{\theta}_{\delta t p}\|_{l^2(J)}^2 \leq \frac{\alpha}{2} \|\boldsymbol{\theta}_{\mathbf{z}}\|_{l^2(L_2)}^2 + \frac{1 + \beta^2 C_c}{2\alpha} \|\boldsymbol{\eta}_{\mathbf{u}t}\|_{l^2(H^1)}^2 + \frac{1}{2\alpha} \|\nabla \cdot \boldsymbol{\eta}_{\mathbf{z}}\|_{l^2(L_2)}^2 \\
& + \frac{\lambda_{min}^{-2} \beta^2}{2\alpha} \|\nabla \cdot \boldsymbol{\eta}_{\mathbf{z}t}\|_{l^2(L_2)}^2 + \frac{1 + \beta^2}{2\alpha} \|\eta_{pt}\|_{l^2(J)}^2 + \frac{(1 + \beta^2 C_c) \Delta t^2}{2\alpha} \|\nabla \cdot \boldsymbol{\eta}_{\mathbf{u}tt}\|_{L^2(L_2)}^2 \\
& + \frac{\lambda_{min}^{-2} \beta^2 \Delta t^2}{2\alpha} \|\boldsymbol{\eta}_{\mathbf{z}tt}\|_{L^2(L_2)}^2 + \frac{(1 + \beta^2) \Delta t^2}{2\alpha} \left(\|\eta_{p_{tt}}\|_{L^2(J)}^2 + \|p_{tt}\|_{L^2(J)}^2 + \|\nabla \cdot \mathbf{u}_{tt}\|_{L^2(L_2)}^2 \right).
\end{aligned}$$

Now choosing α sufficiently small, $\beta \geq \max \left[\frac{C_p}{\alpha C_k} + \frac{C_c \alpha}{2C_k}, \frac{1}{2\alpha} + \frac{3\alpha}{2} \right]$, and applying a discrete version of Gronwall's lemma, we get

$$\begin{aligned}
& \|\boldsymbol{\theta}_{\delta t \mathbf{u}}\|_{l^2(H^1)}^2 + \|\boldsymbol{\theta}_{\mathbf{z}}^N\|_{0,\Omega}^2 + \|\nabla \cdot \boldsymbol{\theta}_{\mathbf{z}}\|_{l^2(L_2)}^2 + \|\boldsymbol{\theta}_{\delta t p}\|_{l^2(J)}^2 \\
& \leq C \left(\|\boldsymbol{\eta}_{\mathbf{u}t}\|_{l^2(H^1)}^2 + \|\nabla \cdot \boldsymbol{\eta}_{\mathbf{z}}\|_{l^2(L_2)}^2 + \|\nabla \cdot \boldsymbol{\eta}_{\mathbf{z}t}\|_{l^2(L_2)}^2 + \|\eta_{pt}\|_{l^2(J)}^2 + \|\boldsymbol{\eta}_{\mathbf{z}}\|_{l^2(L_2)}^2 \right) \\
& + C \Delta t^2 \left(\|\nabla \cdot \boldsymbol{\eta}_{\mathbf{u}tt}\|_{L^2(L_2)}^2 + \|\boldsymbol{\eta}_{\mathbf{z}tt}\|_{L^2(L_2)}^2 + \|\eta_{p_{tt}}\|_{L^2(J)}^2 \right) + C \Delta t^2 \left(\|p_{tt}\|_{L^2(J)}^2 + \|\nabla \cdot \mathbf{u}_{tt}\|_{L^2(L_2)}^2 \right).
\end{aligned}$$

Applying standard approximation results, using the bound (3.3), and noting that

$\|\boldsymbol{\theta}_{\delta t \mathbf{u}}^n\|_{1,\Omega}^2, \|\boldsymbol{\theta}_{\mathbf{z}}^n\|_{0,\Omega}^2, \|\boldsymbol{\theta}_{\delta t p}^n\|_{0,\Omega}^2 \geq 0$, we are left with

$$\begin{aligned}
\|\nabla \cdot \boldsymbol{\theta}_{\mathbf{z}}^n\|_{l^2(L_2)}^2 & \leq Ch^2 \left(\|\mathbf{u}_t\|_{l^2(H^2)}^2 + \|\nabla \cdot \mathbf{z}\|_{l^2(H^1)}^2 + \|\nabla \cdot \mathbf{z}_t\|_{l^2(H^1)}^2 + \|p_t\|_{l^2(H^1)}^2 + \|\mathbf{z}\|_{l^2(H^1)}^2 \right) \\
& + Ch^2 \Delta t^2 \left(\|\nabla \cdot \mathbf{u}_{tt}\|_{L^2(H^1)}^2 + \|\mathbf{z}_{tt}\|_{L^2(H^1)}^2 + \|p_{tt}\|_{L^2(H^1)}^2 \right) \\
& + C \Delta t^2 \left(\|p_{tt}\|_{L^2(J)}^2 + \|\nabla \cdot \mathbf{u}_{tt}\|_{L^2(J)}^2 \right).
\end{aligned}$$

Taking the square root on both sides completes the proof. \square

Theorem 4.5. *Assume that the true solution $(\mathbf{u}, \mathbf{z}, p)$ is in $H^2 \left([H^2(\Omega)]^d \right) \times H^1 \left([H^2(\Omega)]^d \right) \cap H^2 \left([H^1(\Omega)]^d \right) \times H^2 \left(H^1(\Omega) \cap L^2 \right)$, then the finite element solution (3.1) satisfies the error estimate*

$$\|\mathbf{u} - \mathbf{u}_h\|_{l^\infty(H^1)} + \|\nabla \cdot (\mathbf{z} - \mathbf{z}_h)\|_{l^2(L_2)} + \|\mathbf{z} - \mathbf{z}_h\|_{l^2(L_2)} + \|p - p_h\|_{l^\infty(L^2)} \leq C(h + \Delta t).$$

Proof. As previously mentioned we can write the error as $\mathbf{u}^n - \mathbf{u}_h^n = (\mathbf{u}^n - \pi_h \mathbf{u}^n) + (\pi_h \mathbf{u}^n - \mathbf{u}_h^n) = \boldsymbol{\eta}_{\mathbf{u}}^n + \boldsymbol{\theta}_{\mathbf{u}}^n$, and similarly for the other variables. Using lemma 4.2 we can bound the interpolation errors, and using lemma 4.3 and lemma 4.4 we can bound the auxillary errors to give the desired result. \square

5 Numerical Results

In this section, we present both two-dimensional and three-dimensional numerical experiments with analytical solutions to verify the theoretical convergence rates of the fully-discrete finite element method developed in this paper. We also test our method on the popular 2D cantilever bracket problem to make sure our method is able to overcome spurious pressure oscillations often experienced in poroelastic simulations. Finally, a 3D unconfined compression problem is presented that highlight the added mass effect of the method for different choices of the stabilization parameter δ .

5.1 Implementation

For the implementation we used the C++ library libmesh [22], and the multi-frontal direct solver mumps [1] to solve the resulting linear system. To solve the full Biot model problem (1.1), we need to solve the following linear system at each time step:

$$\begin{bmatrix} \mathbf{A} & 0 & \alpha \mathbf{B}^T \\ 0 & \mathbf{M} & \mathbf{B}^T \\ \alpha \mathbf{B} & \Delta t \mathbf{B} & c_0 \mathbf{Q} + \mathbf{J} \end{bmatrix} \begin{bmatrix} \mathbf{u}^n \\ \mathbf{z}^n \\ \mathbf{p}^n \end{bmatrix} = \begin{bmatrix} \mathbf{f} \\ \mathbf{b} \\ \Delta t \mathbf{q} + \mathbf{B} \mathbf{u}^{n-1} + c_0 \mathbf{Q} \mathbf{p}^{n-1} + \mathbf{J} \mathbf{p}^{n-1} \end{bmatrix},$$

where we have defined the following matrices:

$$\mathbf{A} = [\mathbf{a}_{ij}], \quad \mathbf{a}_{ij} = \int_{\Omega} 2\mu_s \nabla \phi_i : \nabla \phi_j + \lambda (\nabla \cdot \phi_i) (\nabla \cdot \phi_j),$$

$$\mathbf{M} = [\mathbf{m}_{ij}], \quad \mathbf{m}_{ij} = \int_{\Omega} \kappa^{-1} \phi_i \cdot \phi_j,$$

$$\mathbf{B} = [\mathbf{b}_{ij}], \quad \mathbf{b}_{ij} = - \int_{\Omega} \psi_i \nabla \cdot \phi_j,$$

$$\mathbf{Q} = [\mathbf{q}_{ij}], \quad \mathbf{q}_{ij} = \int_{\Omega} \psi_i \cdot \psi_j,$$

$$\mathbf{J} = [\mathbf{j}_{ij}], \quad \mathbf{j}_{ij} = \delta \sum_K \int_{\partial K \setminus \partial \Omega} h_{\partial K} [\psi_i] [\psi_j] \, ds.$$

Here ϕ_i are vector valued linear basis functions such that the displacement vector can be written as $\mathbf{u}^n = \sum_{i=1}^{n_u} \mathbf{u}_i^n \phi_i$, with $\sum_{i=1}^{n_u} \mathbf{u}_i^n \phi_i \in \mathbf{W}_h^E$. Similarly for the relative fluid vector we have $\mathbf{z}^n = \sum_{i=1}^{n_z} \mathbf{z}_i^n \phi_i$, with $\sum_{i=1}^{n_z} \mathbf{z}_i^n \phi_i \in \mathbf{W}_h^D$. The scalar valued constant basis functions ψ_i are used to approximate the pressure, such that $\mathbf{p}^n = \sum_{i=1}^{n_p} p_i^n \psi_i$, with $\sum_{i=1}^{n_p} p_i^n \psi_i \in Q_h$.

5.2 2D convergence study

We adapt a test problem used in [9] to verify the convergence of our method. To simplify the analytical solution we have slightly simplified the original Biot system of equations (1.1), by removing material parameters and replacing the linear elasticity equation with the Stokes momentum equation. This simplified system of equations (5.1), retains all the analytical properties and difficulties of the original problem, and any conclusions drawn from this convergence study therefore also apply to the original system of equations (1.1). The analytical solution of the pressure is given by $p = \sin(2\pi x) \sin(2\pi y) \sin(2\pi t)$, with $t \in [0, 0.25]$. For this test problem the domain, Ω , is the unit

square, with boundary $\partial\Omega = \Gamma_d$ for the mixture, and $\partial\Omega = \Gamma_f$ for the fluid. Thus, the simplified system of equations is given by

$$-\nabla^2 \mathbf{u} + \nabla p = 0 \quad \text{in } \Omega, \quad (5.1a)$$

$$\mathbf{z} + \nabla p = 0 \quad \text{in } \Omega, \quad (5.1b)$$

$$\nabla \cdot (\mathbf{u}_t + \mathbf{z}) = g \quad \text{in } \Omega, \quad (5.1c)$$

$$\mathbf{u}(t) = \mathbf{u}_D \quad \text{on } \Gamma_d, \quad (5.1d)$$

$$\mathbf{z}(t) \cdot \mathbf{n} = q_D \quad \text{on } \Gamma_f, \quad (5.1e)$$

$$\mathbf{u}(0) = 0 \quad \text{in } \Omega, \quad (5.1f)$$

where the displacement boundary condition, the fluid flux boundary condition, and the source term are calculated to be

$$\mathbf{u}_D = \begin{pmatrix} -\frac{1}{4}\pi \cos(2\pi x) \sin(2\pi y) \sin(2\pi t) \\ -\frac{1}{4}\pi \sin(2\pi x) \cos(2\pi y) \sin(2\pi t) \end{pmatrix},$$

$$q_D = \begin{pmatrix} -2\pi \cos(2\pi x) \sin(2\pi y) \sin(2\pi t) \\ -2\pi \sin(2\pi x) \cos(2\pi y) \sin(2\pi t) \end{pmatrix} \cdot \mathbf{n},$$

$$g = 2\pi \sin(2\pi x) \sin(2\pi y) \cos(2\pi t) + 8\pi^2 \sin(2\pi x) \sin(2\pi y) \sin(2\pi t).$$

Figure 1 illustrates what happens when the stabilization parameter δ is not chosen large enough ($\delta = 0.1$), resulting in a spurious pressure solution. For this test problem we have found that a value of $\delta = 1$ is sufficiently large to result in a smooth pressure solution (see Figure 1). The value of δ required to produce a stable solution depends on the geometry and material parameters of the particular problem under investigation, but is independent of any mesh parameters. In Figure 2, we show the convergence of the method in relevant norms for each variable, with $\delta = 1, 10, 100$. The rates of convergence agree with the theoretically derived error estimates. Figure 3 and Figure 4 show the deformation, pressure, and fluid velocity in the x and y directions at time $t = 0.125$ and $t = 0.25$, respectively.

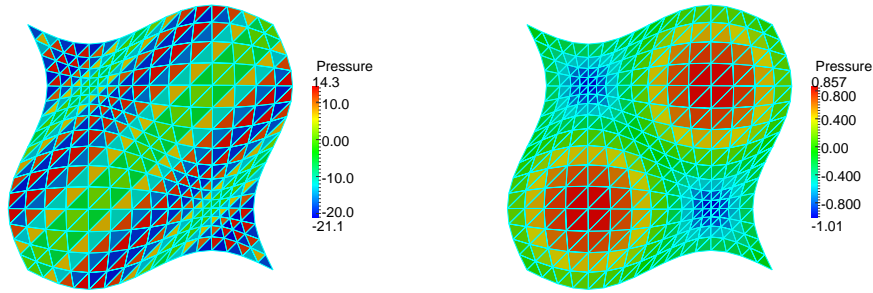


Figure 1: Unstable pressure field (left), caused by not choosing the stabilization parameter δ large enough, with $\delta = 0.1$, at $t = 0.25$. Stable pressure field (right), with $\delta = 1$, at $t = 0.25$.

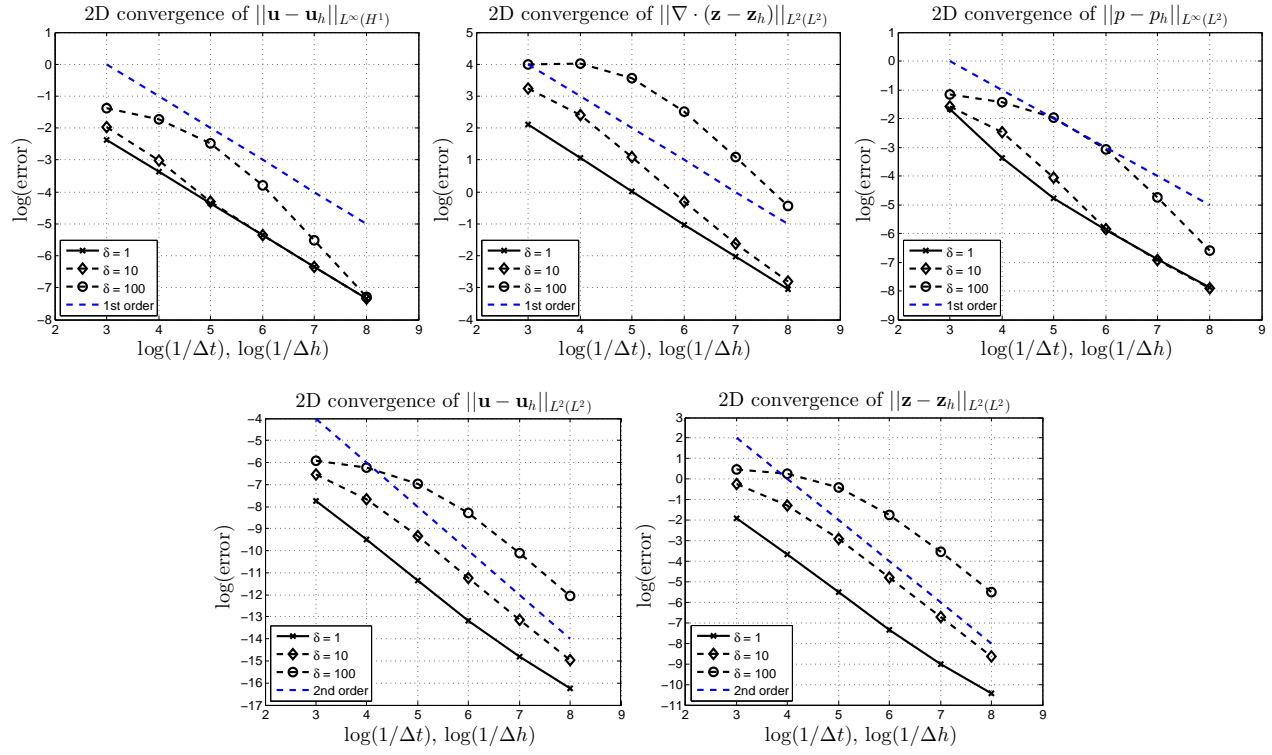


Figure 2: Convergence of the displacement, velocity, and pressure errors in their respective norms of the simplified poroelastic 2D test problem with different stable values of the stabilization parameter δ .

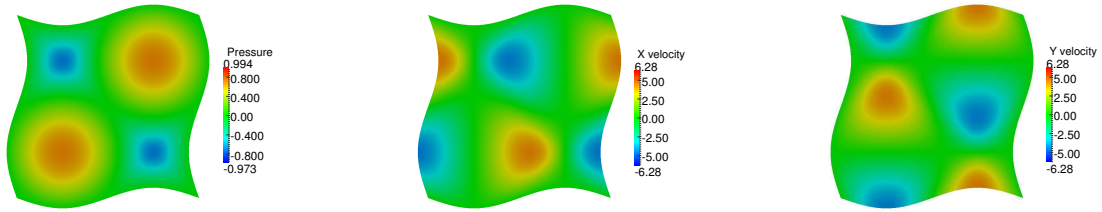


Figure 3: Pressure (left), x -velocity (middle), and y -velocity (right), at $t = 0.125$.

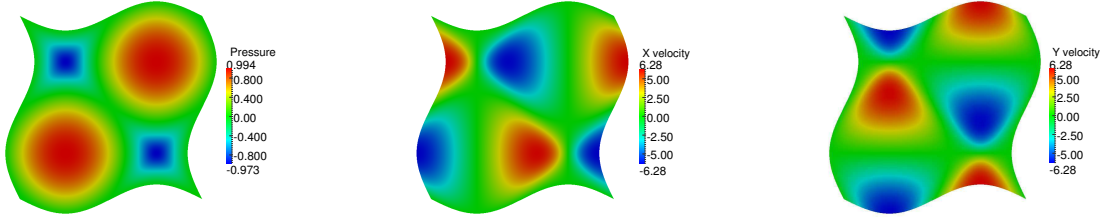


Figure 4: Pressure (left), x -velocity (right), and y -velocity (middle), at $t = 0.25$.

5.3 3D convergence study

We extend the previous test problem to a unit cube. We now set the analytical pressure to $p = \sin(2\pi x) \sin(2\pi y) \sin(2\pi z) \sin(2\pi t)$, which gives the following displacement boundary condition, fluid flux boundary condition, and right hand side source term

$$\mathbf{u}_D = \begin{pmatrix} -\frac{1}{6}\pi \cos(2\pi x) \sin(2\pi y) \sin(2\pi z) \sin(2\pi t) \\ -\frac{1}{6}\pi \sin(2\pi x) \cos(2\pi y) \sin(2\pi z) \sin(2\pi t) \\ -\frac{1}{6}\pi \sin(2\pi x) \sin(2\pi y) \cos(2\pi z) \sin(2\pi t) \end{pmatrix},$$

$$\mathbf{q}_d = \begin{pmatrix} -2\pi \cos(2\pi x) \sin(2\pi y) \sin(2\pi z) \sin(2\pi t) \\ -2\pi \sin(2\pi x) \cos(2\pi y) \sin(2\pi z) \sin(2\pi t) \\ -2\pi \sin(2\pi x) \sin(2\pi y) \cos(2\pi z) \sin(2\pi t) \end{pmatrix} \cdot \mathbf{n},$$

$$g = 2\pi \sin(2\pi x) \sin(2\pi y) \sin(2\pi z) \cos(2\pi t) + 12\pi^2 \sin(2\pi x) \sin(2\pi y) \sin(2\pi z) \sin(2\pi t).$$

In Figure 5, we show the 3D convergence of the method in relevant norms for each variable, with $\delta = 0.001, 0.01, 0.1$. The rates of convergence agree with the theoretically derived error estimates. We have observed that for 3D problems δ can be chosen to be very small compared to 2D problems, making the effect of the stabilization term negligible to the system. This can be explained by the improved ratio of solid displacement and fluid flux nodes to pressure nodes in 3 dimensions, easing the LBB condition, the violation of which explains the spurious pressure oscillations found in unstable finite element formulations.

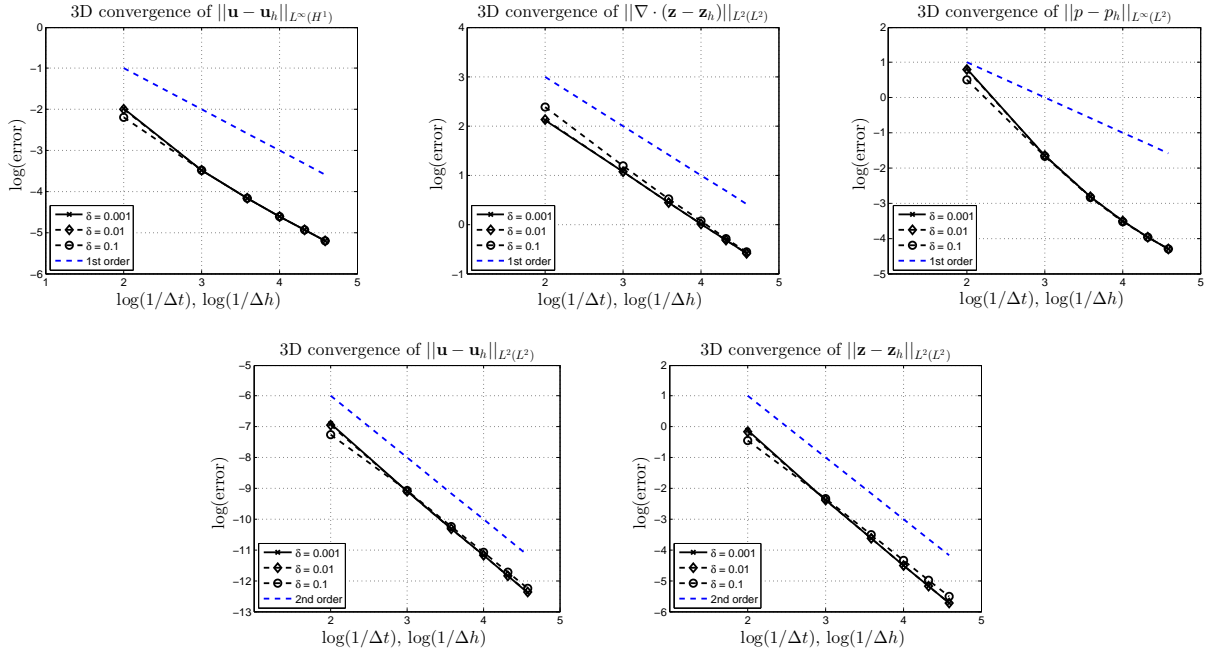


Figure 5: Convergence of the displacement, velocity, and pressure errors in their respective norms of the simplified poroelastic 3D test problem with different stable values of the stabilization parameter δ .

5.4 2D cantilever bracket problem

It has been shown in [33] that continuous Galerkin methods (CG/mixed) developed in [30] and [31] are susceptible to spurious pressure oscillations. As a result various methods which approximate the displacement using discontinuous and nonconforming elements have been proposed to overcome this problem [24],[32],[26],[42]. The cause of this has been attributed to a phenomenon called ‘locking’ in [33]. Phillips et al. [33] give a discussion of locking in poroelasticity and show how it relates to the locking phenomenon found in plane linear elasticity problems. A more recent paper by Haga et al. [18] also investigates the cause of these pressure oscillations, they suggest that for low permeabilities the pressure oscillations are caused by a violation of the inf-sup (LBB) condition. In this example, we consider the 2D cantilever bracket problem. The same test problem has also been used in [33] to showcase the problem of spurious pressure oscillation, and used in [26] and [42] to demonstrate that their method is able to overcome these spurious pressure oscillations. The cantilever bracket problem (shown in Fig. 6a) is solved on a unit square $[0, 1]^2$. No-flow flux boundary conditions are applied along all sides, the deformation is fixed ($\mathbf{u} = 0$) along the left hand-side ($x = 0$), and a downward traction force is applied along the top edge ($y = 1$). The right and bottom sides are traction-free. For this numerical experiment, we set $\Delta t = 0.001$, $h = 1/96$, $\delta = 5e - 6$, and choose the same material parameters as in [33] that typically cause locking: $E = 1e + 5$, $\nu = 0.4$, $\alpha = 0.93$, $c_0 = 0$, $\kappa = 1e - 7$. The proposed stabilized finite element method yields a smooth pressure solution without any oscillations as is shown in Fig. 6b.

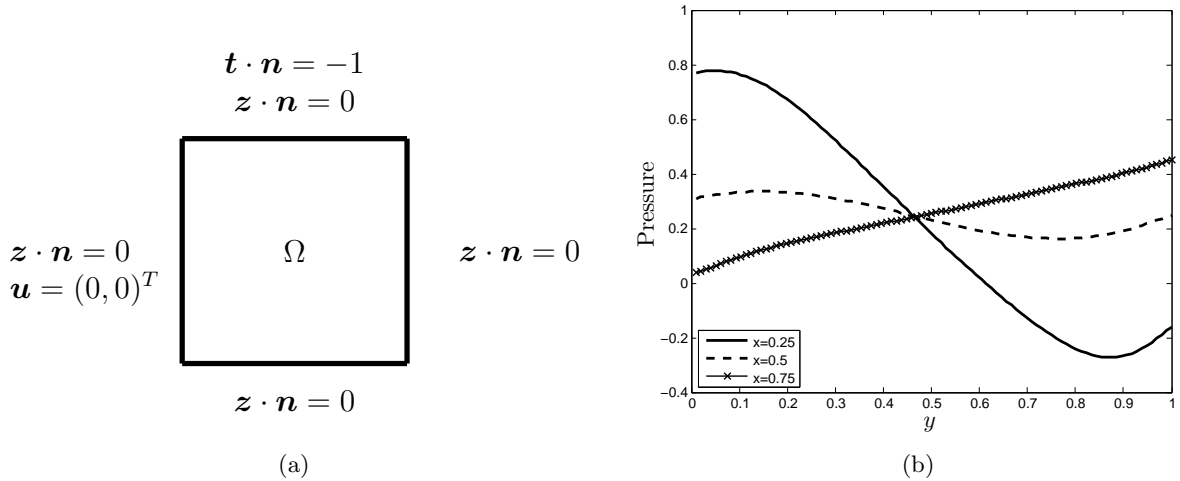


Figure 6: Boundary conditions for the cantilever bracket problem (a). Pressure solution of the cantilever bracket problem at $t = 0.005$ (b).

5.5 3D unconfined compression stress relaxation

In this test, a cylindrical specimen of porous tissue is exposed to a prescribed displacement in the axial direction while left free to expand radially. The original experiment involved a specimen of articular cartilage being compressed via impervious smooth plates as shown in Figure 7a, note that the two plates are not explicitly modelled in the simulation, but are realised through displacement boundary conditions. After loading the tissue, the displacement is held constant while the tissue under the displacement relaxes in the radial direction due to interstitial fluid flow through the material and the frictionless plates. For the porous tissue, the outer radial boundary is permeable and free-draining, the upper and lower fluid boundaries are impermeable and have a no flux condition imposed. The outer radius and height of the cylinder is $5mm$, whereas the axial compression is $0.01mm$. The bottom of the tissue is constrained in the vertical direction. The fluid pressure was constrained to zero at the outer radial surface. The parameters used for the simulation can be found in Table 2. The material parameters μ_s and λ can be related to the more familiar Young's modulus E and the Poisson ratio ν by $\mu_s = \frac{E}{2(1+\nu)}$ and $\lambda = \frac{E\nu}{(1+\nu)(1-2\nu)}$. For the special case of a cylindrical geometry and assumptions regarding the direction of the fluid flow, Armstrong et al. [2] found a closed-form analytical solution for the radial displacement on the porous medium in response to a step loading function. The analytical solution for the radial displacement to this

Parameter	Description	Value
κ	Dynamic permeability	$10^{-1} \text{ m}^3 \text{ s kg}^{-1}$
ν	Poisson ratio	0.15
E	Young's modulus	$1000 \text{ kg m}^{-1} \text{ s}^{-2}$
Δt	Time step used in the simulation	0.1 s
T	Final time of the simulation	10 s

Table 2: Parameters used for the unconfined compression test problem.

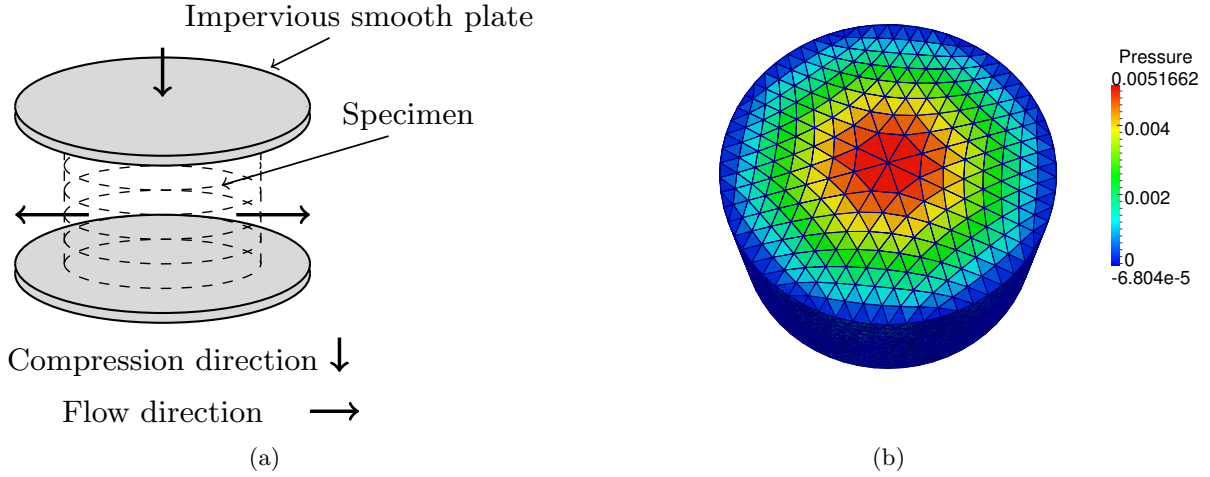


Figure 7: (a) Sketch of the test problem. The porous medium is being compressed via a smooth impervious plate. The frictionless plate permits the porous medium to expand radially, it then gradually relaxes as the fluid seeps out horizontally. (b) Pressure field solution at $t = 5s$, using a mesh with 1227 tetrahedra.

unconfined compression test is given by

$$\frac{u}{a}(a, t) = \epsilon_0 \left[\nu + (1 - 2\nu)(1 - \nu) \sum_{n=1}^{\infty} \frac{\exp(-\alpha_n^2 \frac{H_A k t}{a^2})}{\alpha_n^2 (1 - \nu)^2 - (1 - \nu)} \right]. \quad (5.2)$$

Here α_n are the solutions to the characteristic equation, given by $J_1(x) - (1 - \nu)xJ_0(x)/(1 - 2\nu) = 0$, where J_0 and J_1 are Bessel functions. We also have that ϵ_0 is the amplitude of the applied axial strain, a is the radius of the cylinder, and t_g is the characteristic time of diffusion given by $t_g = a^2/Hk$, where $H = \lambda + 2\mu_s$ is the aggregate modulus of the elastic solid skeleton, and k is the permeability. The radial displacement predicted by our implementation (Figure 8) using a small value of $\delta = 0.001$ shows good agreement with the analytical solution provided by Armstrong et al. [2], and yields a stable solution. The same test problem has also been used to verify other poroelastic software such as FEBio [27]. The analytical solution available for this test problem describes the displacement of the outer radius which is directly dependent on the amount of mass in the system since the porous medium is assumed to be incompressible and fully saturated. It is therefore an ideal test problem for analyzing the effect that the added stabilization term has on the conservation of mass. In Figure 8 we can see that for large values of δ the numerical solution loses mass faster and comes to a steady state that has less mass than the analytical solution. This is a clear limitation of the method and the stability parameter therefore needs to be chosen carefully. However, for 3D problems δ can be chosen to be very small so this effect is negligible, as can be seen in Figure 8 for a stable value of $\delta = 0.001$.

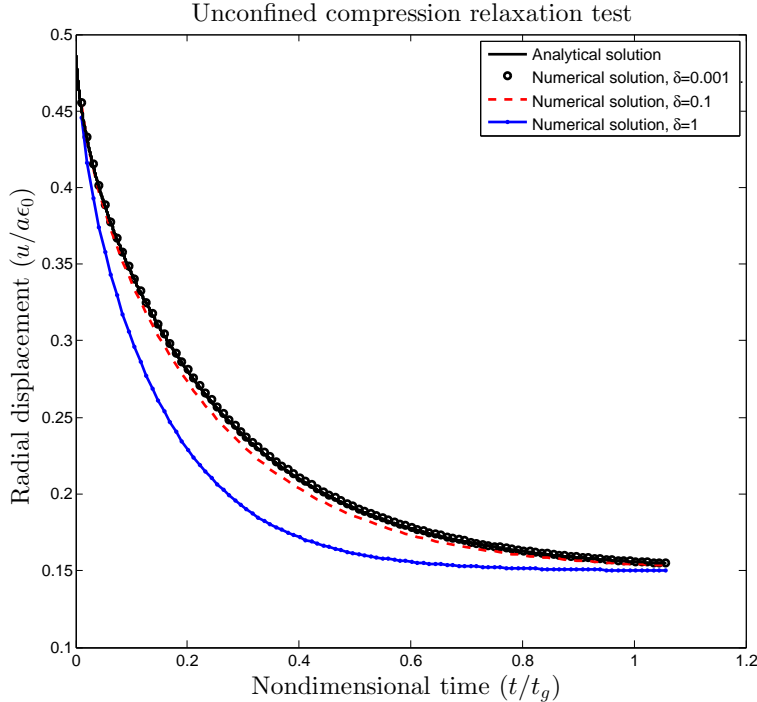


Figure 8: Radial expansion versus time calculated using the analytical solution, and using the proposed numerical method with different values of δ .

6 Conclusion

The main contribution of this paper has been to extend the local pressure jump stabilization method [9], commonly used to solve the Stokes or Darcy equations using piecewise linear approximations for the velocities, and piecewise constant approximations for pressure variable, to three-field poroelasticity. We have presented a stability result for the discretized equations that guarantees the existence of a unique solution of the resulting linear system at each time step, and derived an energy estimate which can be used to prove weak convergence of the discretized system to the continuous problem as the mesh parameters tend to zero. We also derived an optimal error estimate which includes an error for the fluid flux in its natural $Hdiv$ norm. To our knowledge no previous papers have been able to show convergence of a finite element method solving the three-field poroelastic equations in this norm. For practical purposes we have also given a description of the implementation, along with numerical experiments in 2D and 3D that illustrate the convergence of the method, show the effectiveness of the method to overcome spurious pressure oscillations, and evaluate the added mass effect of the stabilization term.

References

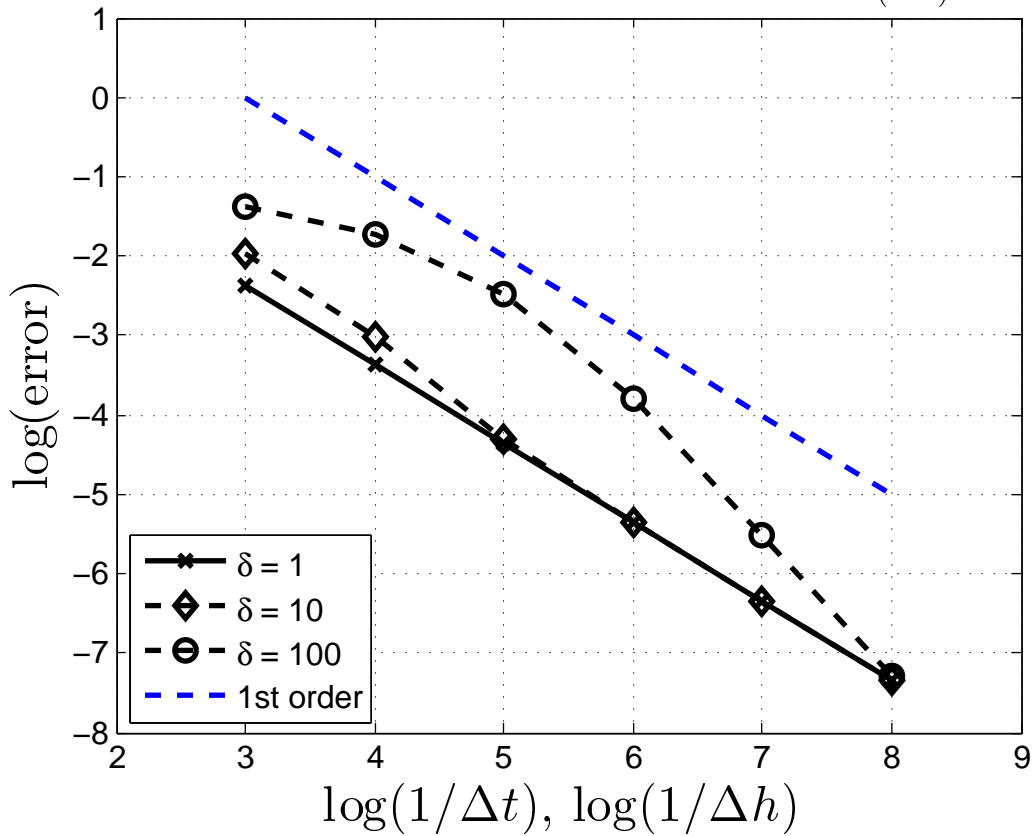
- [1] P.R. Amestoy, I.S. Duff, and J-Y. L'Excellent. Multifrontal parallel distributed symmetric and unsymmetric solvers. *Computer methods in applied mechanics and engineering*, 184(2):501–520, 2000.

- [2] C.G. Armstrong, W.M. Lai, and V.C. Mow. An analysis of the unconfined compression of articular cartilage. *Journal of Biomechanical Engineering*, 106(2):73–165, 1984.
- [3] I. Babuška. Error-bounds for finite element method. *Numerische Mathematik*, 16(4):322–333, 1971.
- [4] S. Badia, A. Quaini, and A. Quarteroni. Coupling Biot and Navier-Stokes equations for modelling fluid-poroelastic media interaction. *Journal of Computational Physics*, 228(21):7986–8014, 2009.
- [5] H. Barucq, M. Madaune-Tort, and P. Saint-Macary. Some existence-uniqueness results for a class of one-dimensional nonlinear Biot models. *Nonlinear Analysis: Theory, Methods & Applications*, 61(4):591–612, 2005.
- [6] P.B. Bochev and C.R. Dohrmann. A computational study of stabilized, low-order C0 finite element approximations of Darcy equations. *Computational Mechanics*, 38(4):323–333, 2006.
- [7] R. Boer. *Trends in continuum mechanics of porous media*, volume 18. Springer, 2005.
- [8] S.C. Brenner and L.R. Scott. *The mathematical theory of finite element methods*, volume 15. Springer, 2008.
- [9] E. Burman and P. Hansbo. A unified stabilized method for Stokes’ and Darcy’s equations. *Journal of Computational and Applied Mathematics*, 198(1):35–51, 2007.
- [10] D. Chapelle, J.F. Gerbeau, J. Sainte-Marie, and I.E. Vignon-Clementel. A poroelastic model valid in large strains with applications to perfusion in cardiac modeling. *Computational Mechanics*, 46(1):91–101, 2010.
- [11] A.N. Cookson, J. Lee, C. Michler, R. Chabiniok, E. Hyde, D.A. Nordsletten, M. Sinclair, M. Siebes, and N.P. Smith. A novel porous mechanical framework for modelling the interaction between coronary perfusion and myocardial mechanics. *Journal of Biomechanics*, 45(5):850 – 855, 2012.
- [12] O. Coussy. *Poromechanics*. John Wiley & Sons Inc, 2004.
- [13] H.C. Elman, D.J. Silvester, and A.J. Wathen. *Finite elements and fast iterative solvers: with applications in incompressible fluid dynamics*. Oxford University Press, USA, 2005.
- [14] X. Feng and Y. He. Fully discrete finite element approximations of a polymer gel model. *SIAM Journal on Numerical Analysis*, 48(6):2186–2217, 2010.
- [15] M. Ferronato, N. Castelletto, and G. Gambolati. A fully coupled 3-D mixed finite element model of Biot consolidation. *Journal of Computational Physics*, 229(12):4813–4830, 2010.
- [16] F. Galbusera, H. Schmidt, J. Noailly, A. Malandrino, D. Lacroix, H.J. Wilke, and A. Shirazi-Adl. Comparison of four methods to simulate swelling in poroelastic finite element models of intervertebral discs. *Journal of the Mechanical Behavior of Biomedical Materials*, 4(7):1234 – 1241, 2011.

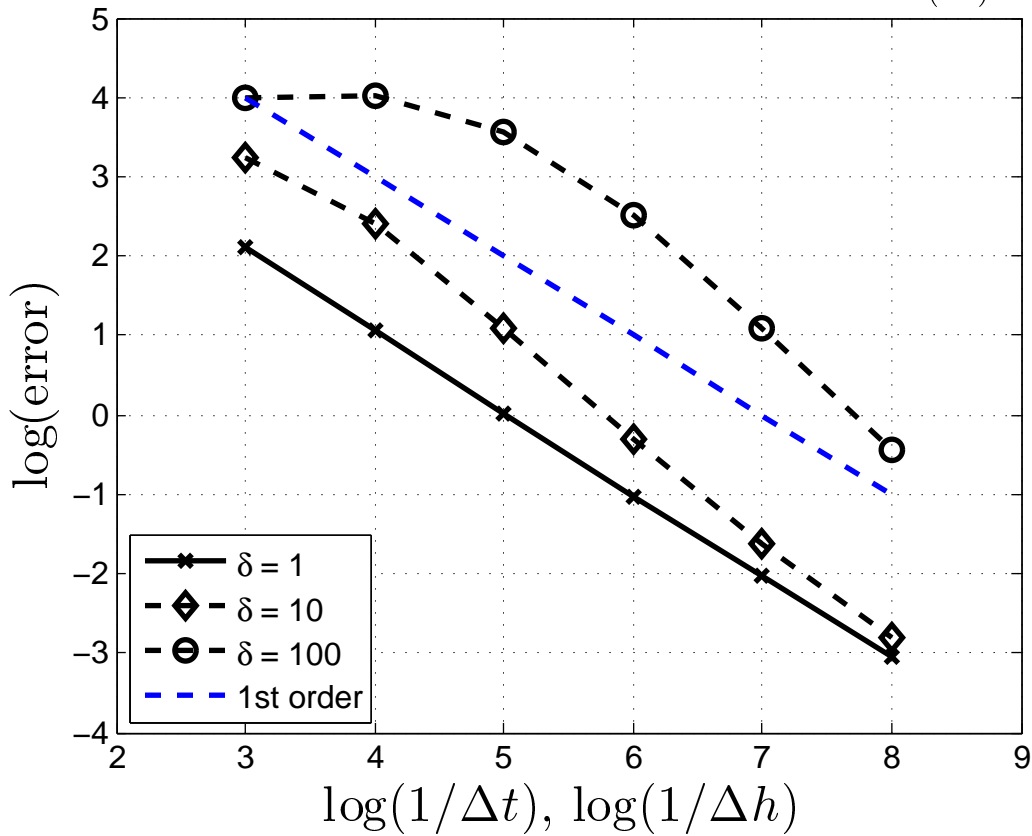
- [17] P.A. Galie, R.L. Spilker, and J.P. Stegeman. A linear, biphasic model incorporating a Brinkman term to describe the mechanics of cell-seeded collagen hydrogels. *Annals of Biomedical Engineering*, 39:2767–2779, 2011.
- [18] J.B. Haga, H. Osnes, and H.P. Langtangen. On the causes of pressure oscillations in low-permeable and low-compressible porous media. *International Journal for Numerical and Analytical Methods in Geomechanics*, 36(12):1507–1522, 2012.
- [19] M.H. Holmes and V.C. Mow. The nonlinear characteristics of soft gels and hydrated connective tissues in ultrafiltration. *Journal of Biomechanics*, 23(11):1145–1156, 1990.
- [20] A.-R.A. Khaled and K. Vafai. The role of porous media in modeling flow and heat transfer in biological tissues. *International Journal of Heat and Mass Transfer*, 46(26):4989–5003, 2003.
- [21] J. Kim, H.A. Tchelepi, and R. Juanes. Stability and convergence of sequential methods for coupled flow and geomechanics: Fixed-stress and fixed-strain splits. *Computer Methods in Applied Mechanics and Engineering*, 200(13):1591–1606, 2011.
- [22] B. S. Kirk, J. W. Peterson, R. H. Stogner, and G. F. Carey. `libMesh`: A C++ Library for Parallel Adaptive Mesh Refinement/Coarsening Simulations. *Engineering with Computers*, 22(3–4):237–254, 2006.
- [23] P. Kowalczyk. Mechanical model of lung parenchyma as a two-phase porous medium. *Transport in Porous Media*, 11(3):281–295, 1993.
- [24] H. Li and Y. Li. A discontinuous Galerkin finite element method for swelling model of polymer gels. *Journal of Mathematical Analysis and Applications*, 398(1):11–25, 2012.
- [25] X.G. Li, H. Holst, J. Ho, and S. Kleiven. Three dimensional poroelastic simulation of brain edema: Initial studies on intracranial pressure. In *World Congress on Medical Physics and Biomedical Engineering*, pages 1478–1481. Springer, 2010.
- [26] R. Liu. *Discontinuous Galerkin finite element solution for poromechanics*. PhD Thesis, The University of Texas at Austin, 2004.
- [27] S.A. Maas, B.J. Ellis, G.A. Ateshian, and J.A. Weiss. FEBio: finite elements for biomechanics. *Journal of biomechanical engineering*, 134(1):1–10, 2012.
- [28] V.C. Mow, S.C. Kuei, W.M. Lai, and C.G. Armstrong. Biphasic creep and stress relaxation of articular cartilage in compression: Theory and experiments. *Journal of Biomechanical Engineering*, 102(1):73–84, 1980.
- [29] M.A. Murad and A.F. Loula. On stability and convergence of finite element approximations of biot’s consolidation problem. *International journal for numerical methods in engineering*, 37(4):645–667, 1994.
- [30] P.J. Phillips and M.F. Wheeler. A coupling of mixed and continuous galerkin finite element methods for poroelasticity i: the continuous in time case. *Computational Geosciences*, 11(2):131–144, 2007.

- [31] P.J. Phillips and M.F. Wheeler. A coupling of mixed and continuous galerkin finite element methods for poroelasticity ii: the discrete-in-time case. *Computational Geosciences*, 11(2):145–158, 2007.
- [32] P.J. Phillips and M.F. Wheeler. A coupling of mixed and discontinuous galerkin finite-element methods for poroelasticity. *Computational Geosciences*, 12(4):417–435, 2008.
- [33] P.J. Phillips and M.F. Wheeler. Overcoming the problem of locking in linear elasticity and poroelasticity: an heuristic approach. *Computational Geosciences*, 13(1):5–12, 2009.
- [34] Alfio Quarteroni. *Numerical models for differential problems*, volume 2. Springer, 2009.
- [35] R.E. Showalter. Diffusion in poro-elastic media. *Journal of mathematical analysis and applications*, 251(1):310–340, 2000.
- [36] V. Thomée. *Galerkin finite element methods for parabolic problems*, volume 25. Springer, 2006.
- [37] R. Verfürth. A posteriori error estimators for convection-diffusion equations. *Numerische Mathematik*, 80(4):641–663, 1998.
- [38] M.F. Wheeler and X. Gai. Iteratively coupled mixed and galerkin finite element methods for poro-elasticity. *Numerical Methods for Partial Differential Equations*, 23(4):785–797, 2007.
- [39] J.A. White and R.I. Borja. Stabilized low-order finite elements for coupled solid-deformation/fluid-diffusion and their application to fault zone transients. *Computer Methods in Applied Mechanics and Engineering*, 197(49):4353–4366, 2008.
- [40] J.A. White and R.I. Borja. Block-preconditioned newton–krylov solvers for fully coupled flow and geomechanics. *Computational Geosciences*, 15(4):647–659, 2011.
- [41] B. Wirth and I. Sobey. An axisymmetric and fully 3D poroelastic model for the evolution of hydrocephalus. *Mathematical Medicine and Biology*, 23(4):363–388, 2006.
- [42] SY. Yi. A coupling of nonconforming and mixed finite element methods for Biot’s consolidation model. *Numerical Methods for Partial Differential Equations*, 29(5):1749–1777, 2013.
- [43] A. Ženíšek. The existence and uniqueness theorem in Biot’s consolidation theory. *Aplikace Matematiky*, 29(3):194–211, 1984.

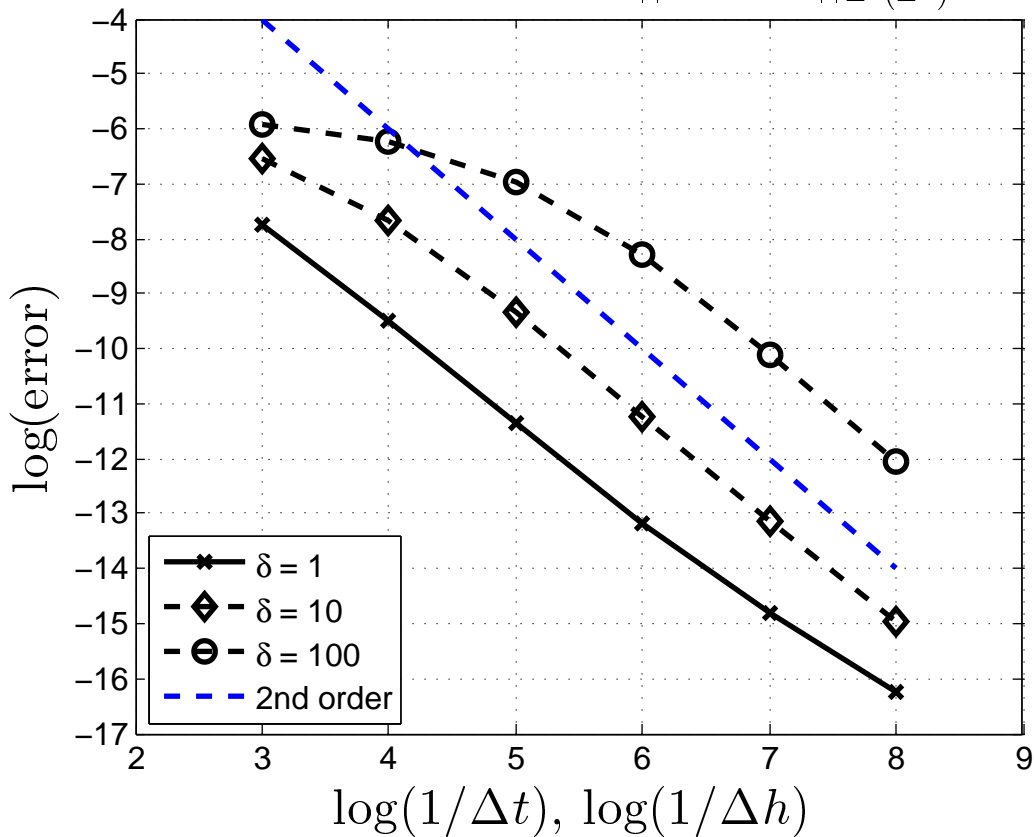
2D convergence of $\|\mathbf{u} - \mathbf{u}_h\|_{L^\infty(H^1)}$



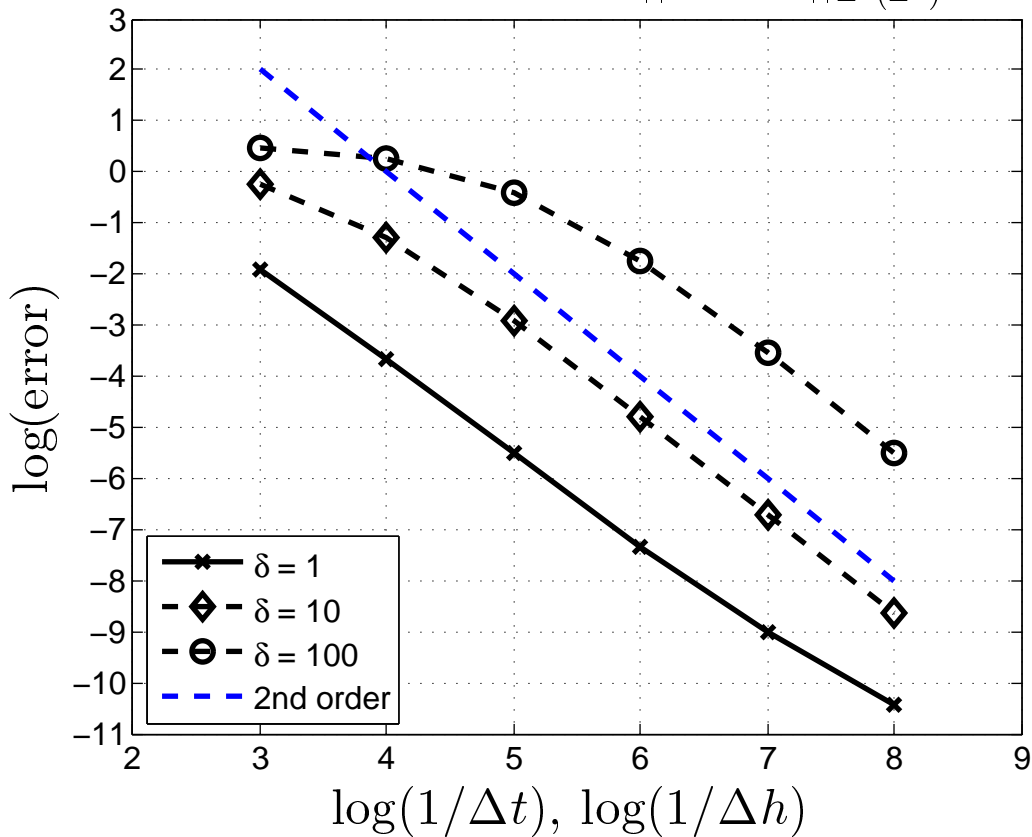
2D convergence of $\|\nabla \cdot (\mathbf{z} - \mathbf{z}_h)\|_{L^2(L^2)}$



2D convergence of $\|\mathbf{u} - \mathbf{u}_h\|_{L^2(L^2)}$



2D convergence of $\|\mathbf{z} - \mathbf{z}_h\|_{L^2(L^2)}$



2D convergence of $\|p - p_h\|_{L^\infty(L^2)}$

